

2023

## Sampling Methods and Transportation analysis of Shipping Containers

Omar Roman-Sanchez  
omararoman20@gmail.com

Follow this and additional works at: <https://huskiecommons.lib.niu.edu/allgraduate-thesesdissertations>



Part of the [Mechanical Engineering Commons](#)

---

### Recommended Citation

Roman-Sanchez, Omar, "Sampling Methods and Transportation analysis of Shipping Containers" (2023).  
*Graduate Research Theses & Dissertations*. 7352.  
<https://huskiecommons.lib.niu.edu/allgraduate-thesesdissertations/7352>

This Dissertation/Thesis is brought to you for free and open access by the Graduate Research & Artistry at Huskie Commons. It has been accepted for inclusion in Graduate Research Theses & Dissertations by an authorized administrator of Huskie Commons. For more information, please contact [jschumacher@niu.edu](mailto:jschumacher@niu.edu).

## ABSTRACT

### SAMPLING METHODS AND TRANSPORTATION ANALYSIS OF SHIPPING CONTAINERS

Omar Roman-Sanchez, MS  
Department of Mechanical Engineering  
Northern Illinois University, 2023  
Nicholas Pohlman, Director

Biomass is a perpetually burgeoning commodity as a sustainable energy resource, but some of the consistent drawbacks are transportation and sampling. The efficiency of pick-up and delivery to conversion facilities needs to be sufficient to allow for longer transport distances. Concurrent work explores the viability of using 20 ft intermodal shipping containers by using a screw auger to pack biomass feedstocks (miscanthus and corn stover) in  $\frac{1}{4}$ -scaled containers, which resulted in dry matter packing densities exceeding  $8 \text{ lb/ft}^3$ . Full analysis of compaction energy plus transportation needs was found to understand net positive energy return on investment. To enhance the sampling capability, two modified shipping containers were designed: one modeled after the  $\frac{1}{4}$  scaled version of the experiments as well as a  $\frac{1}{4}$  scaled model of a standard 20 ft container. Both divided the system into thirds to characterize local density and chemical reactions of pre-treatment processes. Finite element analysis was performed to determine structural integrity of the modified shipping containers. Small-scale 3D printed models were also produced for demonstration purposes. The integration of the energy return-on-investment and modified shipping containers demonstrated further viability of using 20 ft intermodal shipping containers for the next generation bioeconomy.

NORTHERN ILLINOIS UNIVERSITY  
DEKALB, ILLINOIS

AUGUST 2023

SAMPLING METHODS AND TRANSPORTATION ANALYSIS OF SHIPPING  
CONTAINERS

BY

OMAR ROMAN-SANCHEZ  
© 2023 Omar Roman-Sanchez

A THESIS SUBMITTED TO THE GRADUATE SCHOOL  
IN PARTIAL FULFILLMENT OF THE REQUIREMENTS  
FOR THE DEGREE  
MASTER OF SCIENCE

DEPARTMENT OF MECHANICAL ENGINEERING

Thesis Director:  
Nicholas Pohlman

## ACKNOWLEDGEMENTS

I would like to express my gratitude and appreciation to everyone that has contributed to the completion of this thesis. First and foremost, I am immensely grateful to my thesis advisor, Dr. Nicholas Pohlman. His knowledge, insights, and constructive feedback have been instrumental to this thesis. I would like to extend my appreciation to my thesis committee members, Dr. John Shelton and Dr. Mahdi Vaezi, for the time and effort they dedicated to reviewing my work. I would also like to thank the faculty and staff throughout my academic journey for their classes and support that have impacted my academic growth. Finally, I am incredibly thankful to my friends and family for their support, love, and belief in me.

## TABLE OF CONTENTS

	Page
LIST OF FIGURES .....	vi
LIST OF TABLES .....	x
1. INTRODUCTION .....	1
Concurrent Work .....	6
Project Purpose .....	9
2. ENERGY RETURN ON INVESTMENT .....	10
Consumption Energy of Biomass .....	11
Consumption Energy of Fossil Fuels .....	16
Comparison of Energy Sources .....	18
3. MODIFIED SHIPPING CONTAINER .....	22
Modified Shipping Container Design .....	23
Modified Chip Energy Model .....	24
Modified Standard Container Model .....	28
Finite Element Analysis .....	33
3D Printed Scaled Containers .....	44
4. CONCLUSION .....	50

Future Work..... 51

REFERENCES ..... 53

## LIST OF FIGURES

Figure	Page
Figure 1: Energy densities of common fossil fuels and biomass alternatives [2–4].....	2
Figure 2: Two plant seeds after cultivation. a) Corn kernels being loaded into a truck through a combine auger [6], b) Soybeans in and around a burlap sack [7].....	3
Figure 3: U.S. biofuels production since 1981 [8].....	3
Figure 4: Two new sources for biofuel production. a) Miscanthus [9], b) Corn stover [10].....	4
Figure 5: A standard 20ft intermodal shipping container [13].....	5
Figure 6: The North American Intermodal Rail Network showing many railroad routes [14]. ....	6
Figure 7: 1/4-scaled shipping container. ....	7
Figure 8: Loading system used to load biomass feedstocks into 1/4-scaled containers. ....	8
Figure 9: Schematic showing the motor and current sensor measuring one phase. ....	12
Figure 10: Specifications of motor used in concurrent work.....	13
Figure 11: Voltage reading of the motor over the course of the motor running for miscanthus. ..	13
Figure 12: Voltage reading of the motor over the course of the motor running for corn stover. ..	14
Figure 13: Route for transportation energy calculations.....	16
Figure 14: Total energy of each energy source for a 5 ft container.....	19
Figure 15: Energy consumption of each source for transportation and loading. ....	19
Figure 16: Energy-to-transportation and loading ratio of each energy resource. ....	20

Figure 17: Hay bale sampler probe. a) Components of the bale sampler [22], b) Inside of protective shield with cutout of shaft.....	22
Figure 18: Gas powered core sampling kit from AMS, Inc [23]. .....	23
Figure 19: Modified Chip Energy container model. a) Isometric view, b) Front view, c) Top view, d) Side view.....	25
Figure 20: Modified Chip Energy container model with sections opened. ....	26
Figure 21: Corrugation profiles for the modified Chip Energy container. a) Roof, b) Side walls. ....	26
Figure 22: Parts used or suggested in the modified models from McMaster-Carr. a) Blast gate [24], b) Hinge [25], c) Latch [26]. ....	27
Figure 23: Modified standard container model with two views. a) Isometric, b) Front. ....	28
Figure 24: Modified standard container model with different views. a) Top, b) Side, c) Bottom.	29
Figure 25: Modified standard container model with sections opened. ....	29
Figure 26: Corner posts profile for the modified standard container.....	30
Figure 27: Side view of the modified shipping container that shows the placement of the side walls and tube plates (in blue). ....	30
Figure 28: Corner posts region where the end wall is attached. ....	31
Figure 29: Corrugation profile of the side walls for the modified Chip Energy container. ....	32
Figure 30: Profiles for the modified standard container. a) Bottom rails, b) Cross members. ....	33
Figure 31: Properties of the structural steel material from ANSYS. ....	34
Figure 32: Fixed supports for the containers in ANSYS. a) Modified Chip Energy model, b) Modified standard container model. ....	35



Figure 33: Mesh used for the containers in ANSYS. a) Modified Chip Energy model, b) Modified standard container model. ....	35
Figure 34: Janssen pressure equations indicating the decaying exponential form [27].....	36
Figure 35: Equations to calculate the rpm of an auger [29].....	38
Figure 36: Pressure distribution for the modified Chip Energy model.....	39
Figure 37: Pressure distribution for the modified standard container model.....	39
Figure 38: ANSYS results for blast gate slider of the modified Chip Energy model. a) Deformation in the z-direction, b) Equivalent stress of blast gate.....	40
Figure 39: Equivalent stress on the modified Chip Energy container. ....	40
Figure 40: Deformation results of the modified Chip Energy container. a) Front view, b) Isometric view, c) Left side view, d) Right side view.....	41
Figure 41: ANSYS results for blast gate slider of the modified standard container model. a) Deformation in the z-direction, b) Equivalent stress of blast gate.....	42
Figure 42: Equivalent stress on the modified standard container. ....	42
Figure 43: Deformation results of the modified standard container. a) Front view, b) Isometric view, c) Left side view, d) Right side view.....	43
Figure 44: Scaled modified Chip Energy model front view with blast gate off. ....	44
Figure 45: Scaled modified Chip Energy model. a) Top view, b) Side view, c) Opened container top view, d) Opened container side view. ....	45
Figure 46: Scaled modified standard container model. a) Front view, b) Blast gate off view.....	46
Figure 47: Scaled modified standard container model. a) Top view, b) Bottom view.....	46
Figure 48: Scaled modified standard container model. a) Side view, b) Opened container view.	47
Figure 49: Parts used for the scaled models from McMaster-Carr. a) Hinge [30], b) Latch [31].	47

Figure 50: Extrusion added to the side wall of the scaled standard container model for the latch.  
..... 48

Figure 51: Extrusion profile for the scaled containers. a) Chip Energy model (top view), b)  
Standard container model (bottom view)..... 49

## LIST OF TABLES

Table	Page
Table 1: Total Energy for Each Energy Source.....	11
Table 2: Energy Intensity for Each Transportation Mode from Winebrake et. al. [19] .....	15
Table 3: Transportation and Loading Energy for Miscanthus and Corn Stover .....	15
Table 4: Energy Intensity for Each Transportation Mode for Coal from Vanek [20] .....	17
Table 5: Transportation and Loading Energy for Coal and Compressed Natural Gas.....	18
Table 6: Energy-to-Transportation/Loading Ratio for Corn Stover Using Values from Franz [21] .....	21

## CHAPTER 1

### INTRODUCTION

As a burgeoning commodity for sustainable energy, biomass is being explored as a resource to replace fossil fuels. Biomass is a general term for organic materials that come from living or recently dead organisms, including both plants and animals [1]. Common sources of biomass include agricultural leftovers, food crops, grassy/woody plants, and municipal and industrial waste. Biomass has many ways that it can be used for energy, such as being burnt directly to generate heat. Wood has been used for this purpose since early human ancestors. Biomass can be converted directly into electricity through different methods and can also be converted into liquid fuels such as ethanol.

Fossil fuels are organic material, such as plants, that was compressed and heated over millions of years into concentrated solar energy deposits. Lignocellulosic, or plant, biomass, on the other hand, absorbed solar energy to convert carbon dioxide and water into nutrients. The process only occurs over a plant's life cycle, which could be a few months up to many years. This shows why biomass is "renewable", or able to be replenished, unlike fossil fuels which take millions of years to replenish once the supply is used up. Due to the accumulated time of solar energy collection, a method to compare sources of energy is by considering their energy densities. Energy density is a unit of energy per unit of mass/weight, usually given as megajoules (MJ) per kilogram (kg). Prominent fossil fuels such as coal, crude oil, and natural gas have much higher energy densities than biomass feedstocks such as miscanthus, which is a grassy biomass,

and corn stover, which is leftover field remains. The energy densities of biomasses can range from about 16-20 MJ/kg [2–4] while fossil fuel energy densities range from about 24-55 MJ/kg [2], as shown in Figure 1. While fossil fuels are about 2-3 times richer in energy density, biomass fuels are on the order of magnitude to be considered as energy resources. The ability for renewable resources to make up the difference through handling and transportation means that practically carbon neutral biomass can become a burgeoning sustainable energy resource that can replace fossil fuels and their deficiencies of limited supply and carbon emissions.

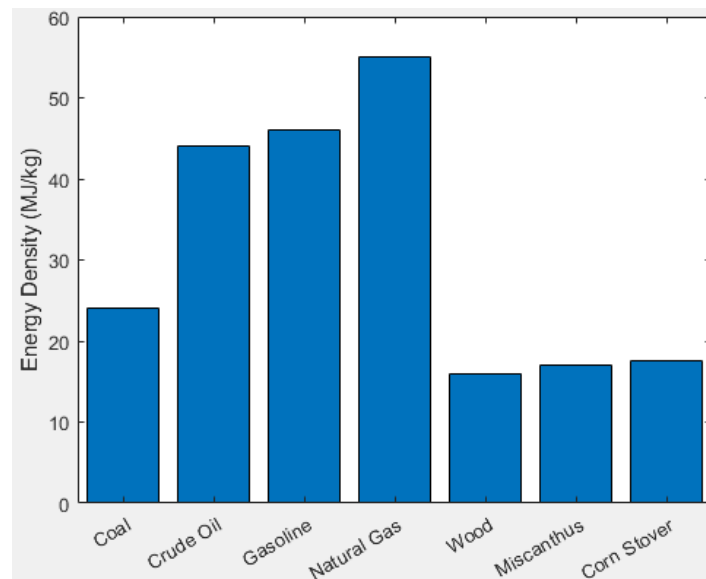


Figure 1: Energy densities of common fossil fuels and biomass alternatives [2–4].

Agriculture involves the cultivation of crops for production of food and plant products. One step in the process of agriculture is the transportation of plant seeds for cultivation, such as corn kernels, wheat kernels, soybeans, and nuts. Typically, seeds are used for food products, but corn kernels and other grains are used in the production of biofuels due to the high starch content in those crops [1,5]. Seeds typically have small, rounded shapes and smooth surfaces as shown in Figure 2. Both aspects enhance the flowability of seeds in agriculture equipment such as augers. Enhanced flowability allows for easier movement and handling of biomass for processing and

transportation. Issues that arise with grains include relatively high fuel, fertilizer, and water consumption as well as needing suitable land for food crops [5]. As a result, the production of biofuels has stagnated. Figure 3 shows that after a significant rise in biofuel production in the 2000s, production seems to be leveling off since 2010.



Figure 2: Two plant seeds after cultivation. a) Corn kernels being loaded into a truck through a combine auger [6], b) Soybeans in and around a burlap sack [7].

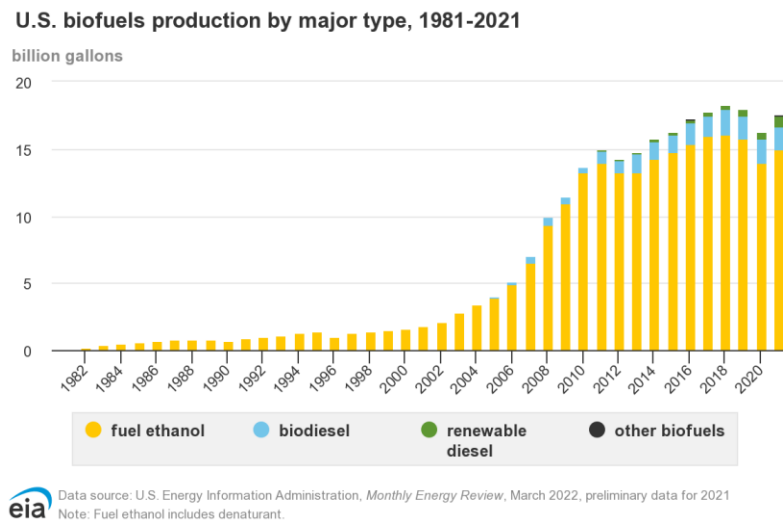


Figure 3: U.S. biofuels production since 1981 [8].

New sources of biofuels such as miscanthus do not consume the same amount as grains and can be grown on land not suitable for food crops. Although corn stover is a byproduct of the corn harvest, it can be used for biofuel production instead of being left as waste. The new biofuels sources can help to increase biofuel production once again, but consistent drawbacks are sampling and transportation. Specifically, sampling while in containers is difficult, and the efficiency of pick-up and delivery to conversion facilities is not sufficient. The reason for these drawbacks is the flowability. Unlike the shapes of seeds as shown in Figure 2, the length and shape of miscanthus and corn stover, as shown in Figure 4, make the flowability difficult resulting in low densification and less overall biomass being transported.



Figure 4: Two new sources for biofuel production. a) Miscanthus [9], b) Corn stover [10].

Biomasses, similar to miscanthus and corn stover, are usually transported in bales that would eventually become livestock bedding. The issues with baling include difficulty in transporting large distances, storing the bales, and losses of biomass in the baling process. One reason for transportation difficulty is the low densities of bales [11]. Round bales are widespread due to availability and low cost of equipment, but difficult to stack and dangerous to transport [11]. Square bales are easier to stack, easier to transport, and have higher densities than round

bales, but the equipment is much more expensive and less widespread. The proposed solution is using intermodal shipping containers to solve the issues of transporting large distances, stacking, and storing.

A standard 20 ft ISO shipping container, as seen in Figure 5, has dimensions of 20 ft long by 8 ft wide by 8 ft high with an inner volume of about 1172 ft<sup>3</sup>. The advantages of these containers are their ability to be moved around and stored easily. Intermodal containers are able to be lifted by forklifts through pockets at the bottom of the container. Containers also have corner castings that are specifically made for easy crane loading and unloading as well as stacking for storage [12]. The large doors of containers allow for easy storage of products inside. The most important aspect is easy transportability as there is infrastructure already in place to transport containers all around the world using trucks, trains, and ships. Figure 6 demonstrates an example of an intermodal network that shows the many different railroads routes that a shipping container can travel through.



Figure 5: A standard 20ft intermodal shipping container [13].



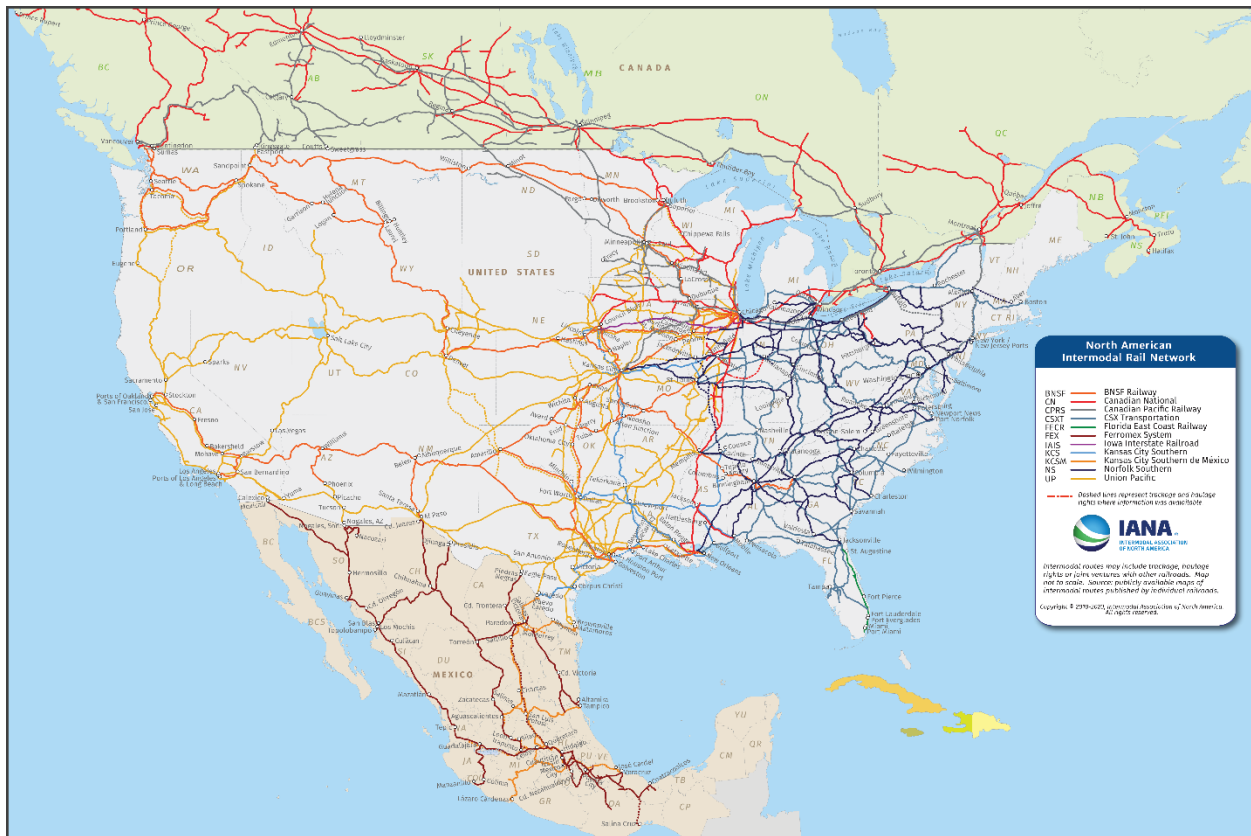


Figure 6: The North American Intermodal Rail Network showing many railroad routes [14].

### Concurrent Work

This thesis is an accompanying project to the funded grant project by the Illinois Innovation Network, “Laboratory-scale biomass containers to achieve transportation density and lignin pre-treatment processes.” This seed project is led by Dr. Pohlman and Dr. Canam from Eastern Illinois University working with Paul Wever, president at Chip Energy, Inc. The handling of biomass with shipping containers and pre-treatment processes on the biomass was tested. Miscanthus and corn stover were the two biomass feedstocks studied with two pre-treatment processes of white rot fungus and calcium hydroxide to breakdown the lignin in the biomasses. Three one-fourth length scaled shipping containers were built for handling and storage as shown

in Figure 7. The volume being about one-sixty fourth of a standard shipping container. These containers allowed for practical testing that extends bench-top capability beyond test tubes and Erlenmeyer flasks.



Figure 7: 1/4-scaled shipping container.

A schematic of the loading system for the containers is shown in Figure 8. The system is set up as an auger connected to a 3 hp three phase power motor through a hopper feeding the biomass through the end caps of the containers. The biomass was shoveled onto a conveyor and sprayed with the pre-treatment chemical for the different trials. The conveyor fed the biomass into the hopper. A current sensor was connected to the motor to detect the motor's current and convert it into a measurable output voltage. The sensor was used to collect energy input and find the time when the auger began jamming as the sensor would show a spike in current consumption of the motor drive when jamming started. Then, the motor would be turned off and weighing of the container would enable calculation of the packing density. Samples would be collected through bung holes in the container or out of the end caps. Material size affected

jamming of the auger and densities of 8-9 pounds per cubic foot ( $\text{lb}/\text{ft}^3$ ) were found which are comparable to bale densities.

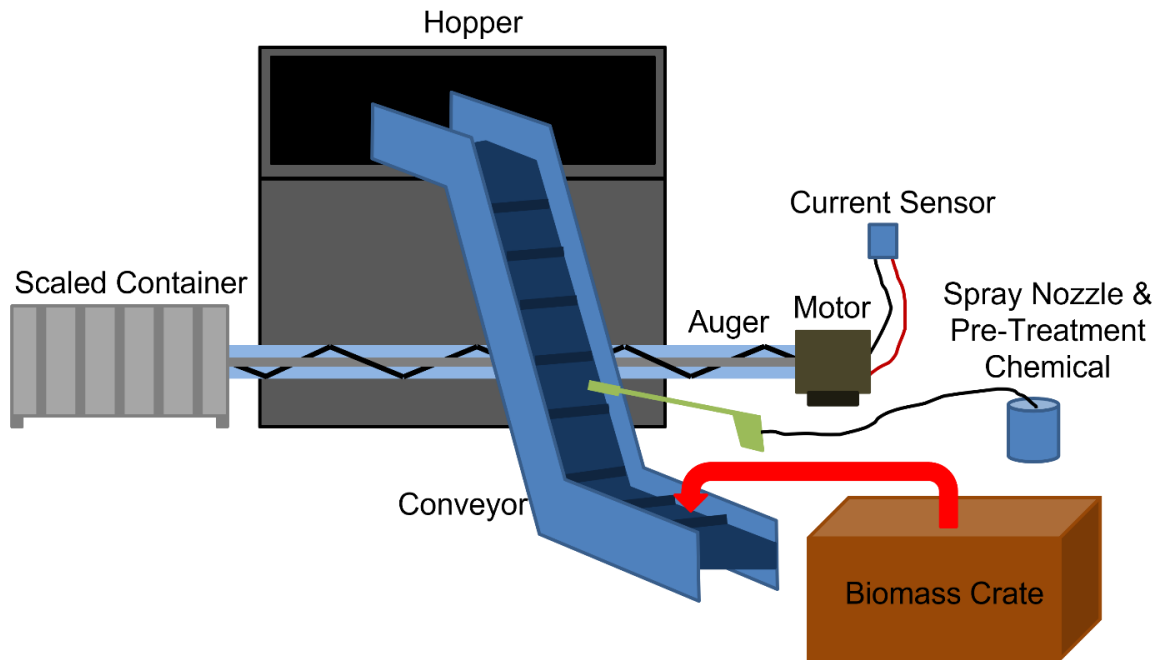


Figure 8: Loading system used to load biomass feedstocks into 1/4-scaled containers.

A previous study was done by Jiskra et. al. [15] to determine the feasibility of using shipping containers to transport biomass with a cost analysis, specifically using Chip Energy's infrastructure. A comparison of round bales, square bales, and shipping containers was done looking at storage, handling, labor, and equipment costs. It was determined that up to \$1.3 million could be saved annually using shipping containers. A reduction of storage space was also determined to be roughly one fourth in total acreage. This study showed the economic feasibility of shipping containers as an alternative to using bales for transportation and storage. Subsequent work in Chapter 2 will demonstrate the system energy consumption by including the loaded energy when compared to fossil fuels. Through the overall source to conversion process, biomass will have to achieve peak efficiency to make up the energy density differences noted in Figure 1.

## Project Purpose

This thesis is intended to help determine the viability of using shipping containers to transport biomass. One component is determining an energy return on investment for using shipping containers. This component is intended to show that biomass is able to compete as an alternative with prevailing fossil fuels in terms of energy investment returns. The other component is creating a modified shipping container to allow for easier sampling in the accompanying project. This component helps to determine which pre-processing treatments allow for lignin breakdown and what the local density is towards the center of the container. Both components will help to further biomass as an important sustainable energy resource.

## CHAPTER 2

### ENERGY RETURN ON INVESTMENT

To understand the viability of using shipping containers to transport biomasses, a return of investment analysis based on energy was developed. A sufficient analysis requires a look at the total energy of the source against the energy consumption of transportation and loading. For this thesis, the energy return on investment will be referred to as energy-to-transportation and loading ratio (ETLR) due to its smaller scope. A comparison between the biomasses (miscanthus and corn stover) and fossil fuels (coal and compressed natural gas) was performed using the modified 5 ft scaled containers from the concurrent work as a basis for total amount. This meant that the volume (21.67 ft<sup>3</sup>) used for analysis was constant for each energy source. Compressed natural gas (CNG) was an exception because the volume (15.71 ft<sup>3</sup>) used was calculated using a natural gas tank of 5 ft length with a diameter of 24 in. since that is the width of the modified concurrent work container. The total energy from each source was calculated using the following equation:

$$E_{src} = V \times \rho \times E_{\rho} \quad (1)$$

where the volume of the container is  $V$ , the density of each energy source is  $\rho$ , and the energy density of the source is  $E_{\rho}$ . The source energy is given in kWh with the subscript “th” that indicates thermal energy potential instead of converted electrical energy potential.

The energy totals for each source, as well as the volumes, densities, and energy densities, are displayed in Table 1. The density for coal was the highest typical bulk density of the most abundant rank of coal: bituminous coal [16]. The natural gas density was found with the low-end pressure of a pipeline (500 psi) at a temperature of 25°C [17]. The bulk density for miscanthus and corn stover that was used is from the concurrent work data. The energy densities are the same as given in Figure 1.

Table 1: Total Energy for Each Energy Source

Energy Source	V (ft <sup>3</sup> )	$\rho$ (kg/m <sup>3</sup> )	$E_{\rho}$ (MJ/kg)	$E_{src}$ (kWh <sub>th</sub> )
Miscanthus	21.67	129.75	17	375.85
Corn Stover	21.67	46.45	17.6	139.31
Coal	21.67	913	24	3734.33
Natural Gas	15.71	24.95	55	169.56

### Consumption Energy of Biomass

Using the data gathered in the concurrent work regarding collecting energy input, the biomass loading energy can be calculated for both miscanthus and corn stover. The motor specifications are shown in Figure 10 which had a gear ratio connection of 25.64 to 1 that turned the auger. The motor was used at the higher voltage of 460 V. Figure 11 and Figure 12 display the voltage recording after measuring the current of the power motor with an AcuAmp sensor over the course of the motor being run for miscanthus and corn stover respectively. A schematic of the motor and sensor is shown in Figure 9. Since the sensor output was chosen to be voltage and has a ratio of 1 A to 1 V, the data can be converted to amps [18]. The maximum rating chosen of the sensor was 10 A which explains a saturation limit of 10 V. To get the total energy

consumption of the motor, the typical power equation for a three-phase motor can be modified by using the integral of the current over the course of time the motor was run displayed in the following equation:

$$E_{load} = \sqrt{3} \times PF \times V_m \times \int_{t_i}^{t_f} I dt \quad (2)$$

where the power factor of the motor is  $PF$ , the voltage of the motor is  $V_m$ , the initial time is  $t_i$ , the final time is  $t_f$ , and the current of the motor is  $I$ .

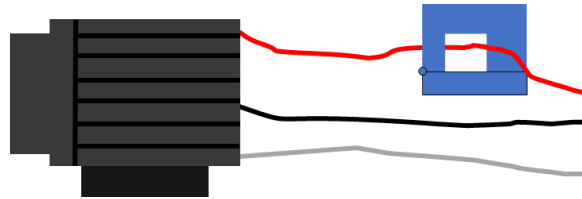


Figure 9: Schematic showing the motor and current sensor measuring one phase.

To find the integral of the current, the data was numerically integrated using the trapezoidal method (trapez function from MATLAB) at the sampling interval of 0.5 seconds. The results for the loading energy for both biomasses are displayed in

Table 3. For corn stover, the loading data has two loadings due to the corn stover intermittently jamming the auger by sticking to the auger with a fully filled hopper. The corn stover had to be hand fed into the hopper instead of completely filling the hopper and then turning on the auger. The intermittent spikes are minor jams, and full compression of the corn stover in the container was not achieved which meant that the density of the corn stover in the container was very low.



Figure 10: Specifications of motor used in concurrent work.

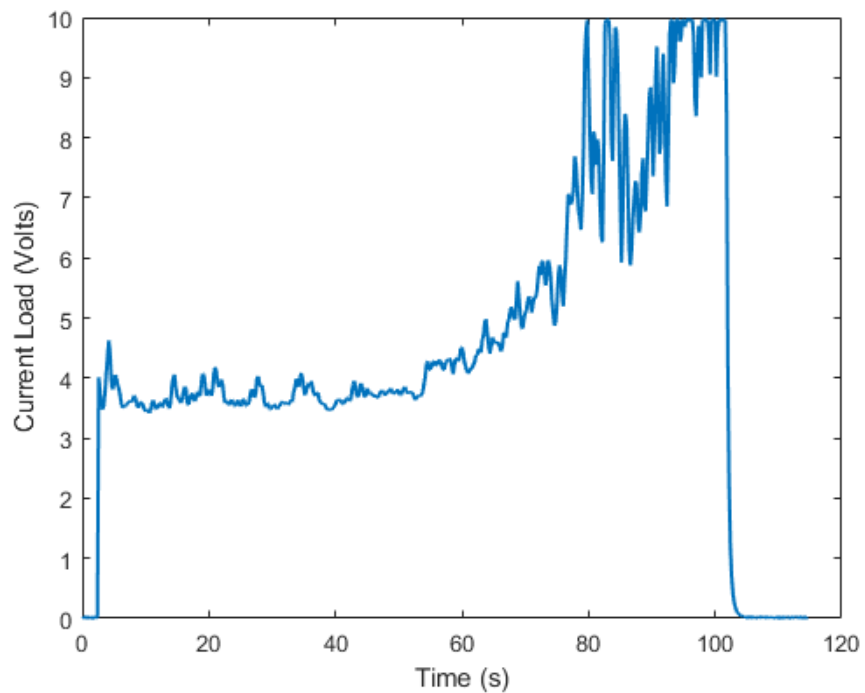


Figure 11: Voltage reading of the motor over the course of the motor running for miscanthus.



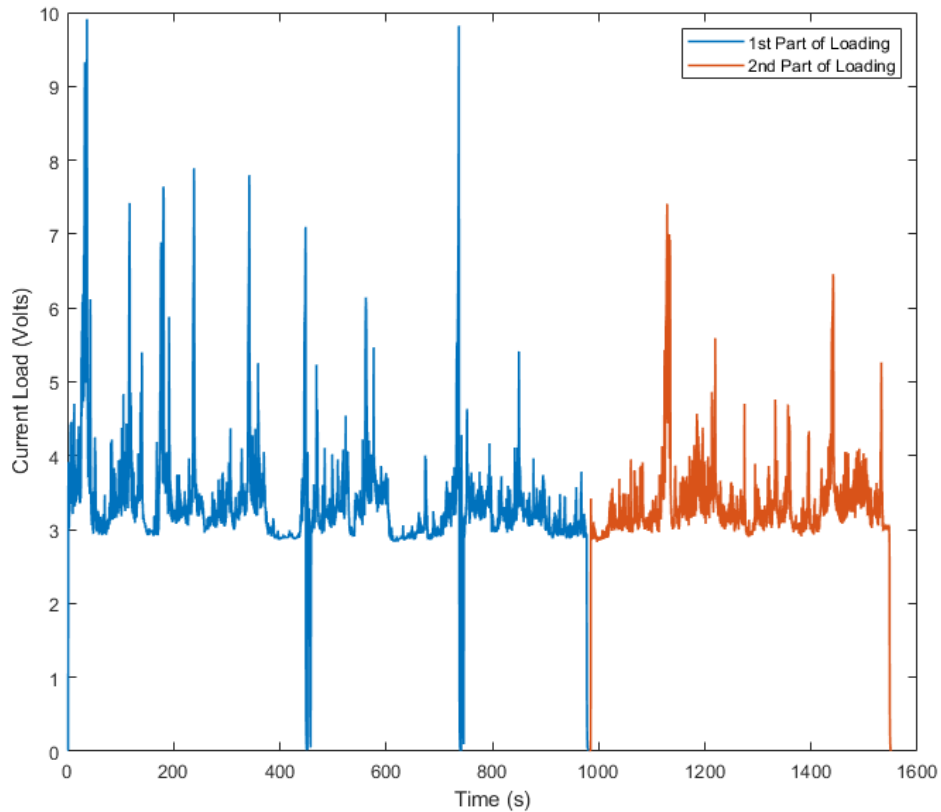


Figure 12: Voltage reading of the motor over the course of the motor running for corn stover.

For transportation energy consumption of miscanthus and corn stover, Winebrake et. al. [19] found the energy input for transportation of goods in shipping containers for three different modes of transportation: truck, rail, and ship. Table 2 shows the energy intensity for each mode in units of Btu/TEU-mile. The unit of TEU stands for 20 ft equivalent unit. Winebrake et. al. describes the TEU unit as “...essentially a volumetric measure (as opposed to weight) and represents the equivalent volume of a 20-ft container” [19]. This means that the energy intensity for each mode can be converted using the internal volume ( $1172 \text{ ft}^3$ ) of a standard 20-ft container. The volumes from Table 1 were used in the calculation. For total distance traveled, a route from DeKalb, IL to Peoria, IL was conceived as illustrated in Figure 13. Total distance traveled by truck was 30 mi, to give a radius of 15 mi around both DeKalb and Peoria. The

Union-Pacific railroad track that travels through DeKalb and Peoria gives a total distance traveled by rail of about 130 mi.

Table 3 displays the transportation energy consumption for miscanthus and corn stover. Rail has the lowest energy intensity with the truck and ship modes having similar intensities. For the route, only the truck and rail mode energy intensities were used and resulted in the same transportation energy for both biomasses as the energy intensities do not take into account the mass of the commodity.

Table 2: Energy Intensity for Each Transportation Mode from Winebrake et. al. [19]

<b>Transportation Mode</b>	<b>Energy Intensity (Btu/TEU-mile)</b>	<b>Converted Energy Intensity (kWh/ft<sup>3</sup>-mile)</b>
Truck	10704	0.0027
Rail	2590	0.0006
Ship	13040	0.0033

Table 3: Transportation and Loading Energy for Miscanthus and Corn Stover

<b>Biomass</b>	<b>E<sub>load</sub> (kWh)</b>	<b>E<sub>trans</sub> (kWh)</b>
Miscanthus	0.0937	3.5642
Corn Stover	0.9369	3.5642

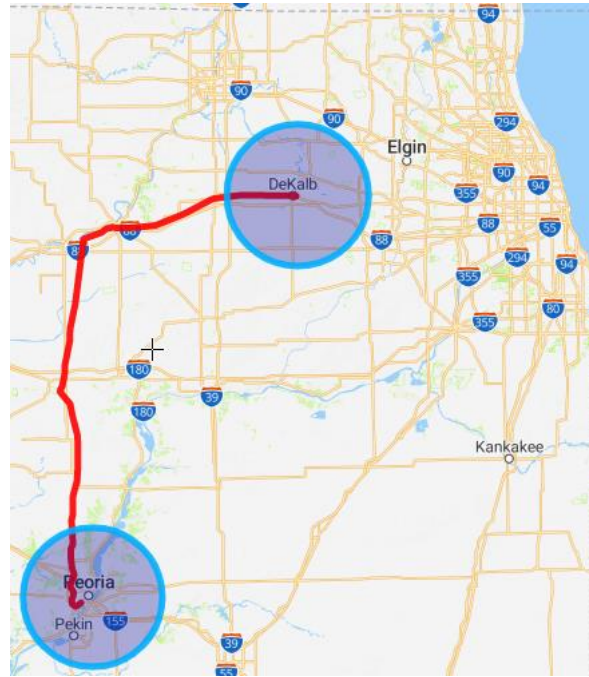


Figure 13: Route for transportation energy calculations.

### Consumption Energy of Fossil Fuels

The loading energy for both fossil fuels is different from the loading energy of the biomasses and from each other. For coal, the simple equation of potential energy is used for loading energy. The reason for using equation (3) is that the energy to load coal in a container (assumed to be open-top and of similar size to the concurrent work containers) can be simplified to the energy needed to lift an amount of coal. This amount is the total mass of coal to fill the container's volume. The height of the container is the distance from the ground to the top of the container which is about 31.5 in. The mass is  $m$ , the gravitational acceleration is  $g$ , and the height of the container is  $h$ .

$$E_{load} = m \times g \times h \quad (3)$$

For compressed natural gas loading energy, a different boundary-work equation can be used, as shown in equation (4). The difference is that the volume stays constant with the pressure undergoing the change. The lower pressure of a compressed natural gas pipeline (500 psi) is used as the final pressure. The initial pressure is gauge pressure of 0 psi. Both pressures have already taken into account the atmospheric pressure. The volume of the natural gas container is  $V$ , the final pressure is  $P_f$ , and the initial pressure is  $P_i$ .

$$E_{load} = V \times (P_f - P_i) \quad (4)$$

The energy intensity for coal of truck and rail transportation is shown in Table 4 given by Vanek [20] using the US Commodity Flow Survey (USCFS). The mass was calculated using the densities and volumes in Table 1. Vanek also gave energy intensity of petroleum/coal products which is the average energy intensity for the commodities of gasoline, diesel, and petroleum/coal products such as gaseous hydrocarbons that includes natural gas in both forms: compressed and liquified. The issue with using Vanek's values for natural gas is that many different commodities being averaged out, so the energy intensity values given by Winebrake et. al. were used instead. Table 5 displays the energy consumption of loading and transportation for both coal and natural gas using the same route demonstrated in Figure 13.

Table 4: Energy Intensity for Each Transportation Mode for Coal from Vanek [20]

<b>Commodity and Transportation Mode</b>	<b>Energy Intensity (Btu/ton-mile)</b>	<b>Converted Energy Intensity (kWh/kg-mile)</b>
Coal (Truck)	2134	$6.8943 \times 10^{-4}$
Coal (Rail)	98	$3.1661 \times 10^{-5}$

Table 5: Transportation and Loading Energy for Coal and Compressed Natural Gas

<b>Fossil Fuel</b>	<b>E<sub>load</sub> (kWh)</b>	<b>E<sub>trans</sub> (kWh)</b>
Coal	0.0012	13.8910
CNG	0.4260	2.5840

### Comparison of Energy Sources

The resulting energy calculations can be used to compare each of the sources of energy and determine the ETLR for each. Figure 14 demonstrates the total energy output for each source using the concurrent work container. Coal has the highest energy output due to the high bulk density of coal compared to the densities of both biomasses and CNG. Miscanthus outperforms corn stover and natural gas but requires about 10 containers to be able to reach the total energy of coal. Corn stover would need about 32 containers to reach the same total energy of coal. The energy inputs are illustrated in Figure 15, which shows that coal consumes the most energy compared to both biomasses and CNG. In fact, CNG shows the least amount of energy consumption, but miscanthus and corn stover are comparable. Corn stover consumed the most loading energy, but this was due to the corn stover sticking to the auger and jamming it. If the corn stover would have flowed more efficiently into the container, the energy might be more comparable to the miscanthus loading energy. The transportation energy shown is for the transportation through the route between DeKalb and Peoria.

Transportation affects the ETLR more significantly than the loading. The ETLR decreases as the transportation distance increases. Since the energy intensity for truck transportation is higher than rail transportation, increasing truck transportation decreases the

ETLR more substantially than rail. This means that rail transportation is more efficient than truck transportation.

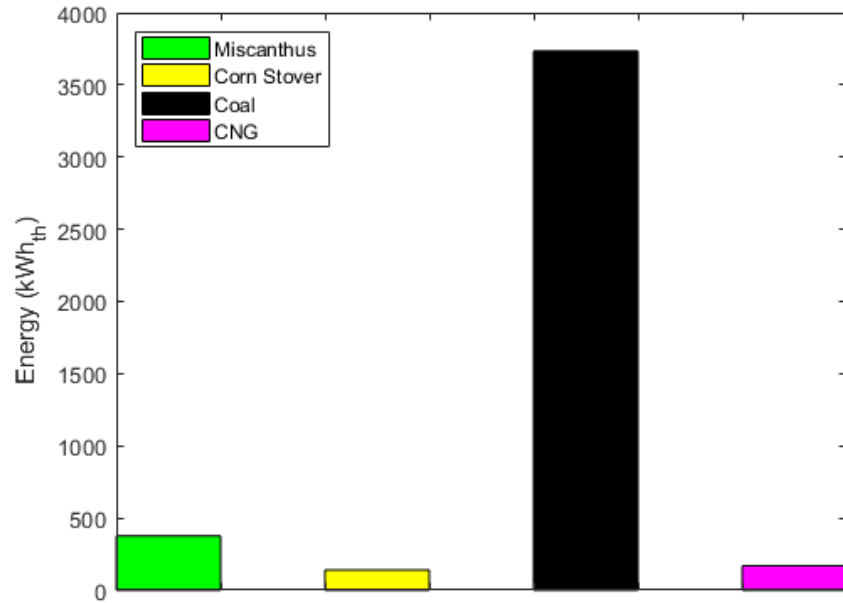


Figure 14: Total energy of each energy source for a 5 ft container.

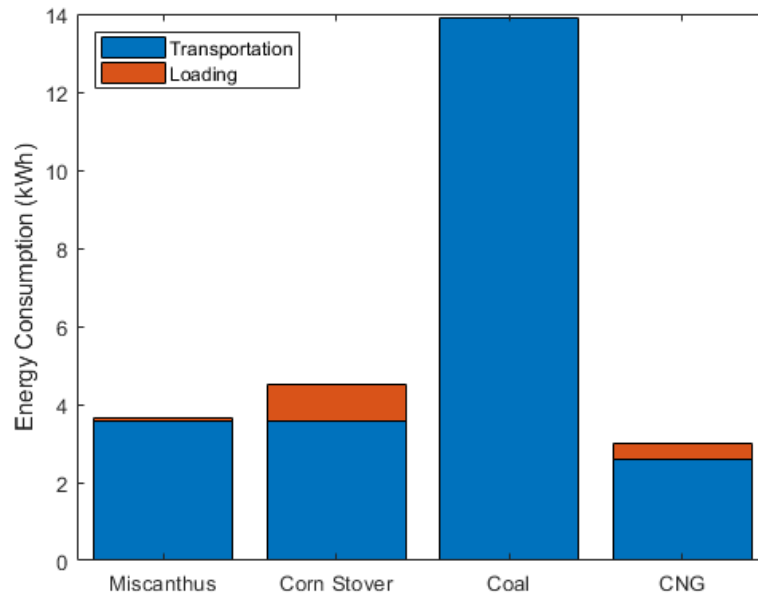


Figure 15: Energy consumption of each source for transportation and loading.

After calculating each the energy inputs and outputs for each energy source, the ETLR for each source can be determined. This is a simple ratio of energy output to energy input, displayed in Figure 16. Although coal shows an ETLR of about 269, miscanthus, with an ETLR of about 103, has the ability to compete with improvements to the loading process. The ETLR of natural gas is low due to using a gas container at standard pipeline pressure instead of using liquefied natural gas which increases the density substantially. This reason is why compressed natural gas is commonly transported by pipeline instead of containers. As previously mentioned, the reason for the persistent use of coal is its high density. If miscanthus density can increase, then miscanthus will be able to approach the ETLR of coal. Even just doubling the density of miscanthus gets an ETLR of about 200, but this does not account for energy consumption from loading to acquire that density.

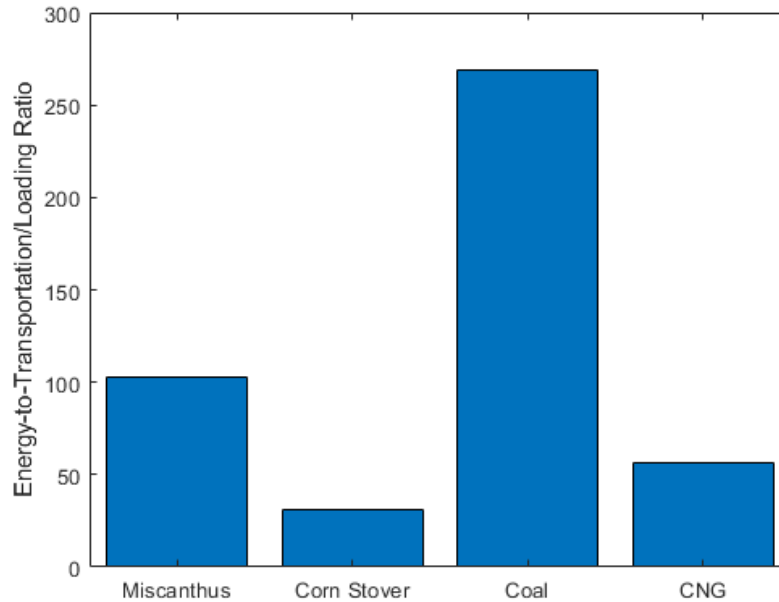


Figure 16: Energy-to-transportation and loading ratio of each energy resource.

The corn stover is shown to have a low return on investment of 31, but increasing the density increases the return on investment just as the miscanthus. Franz [21] gives the values for

corn stover density and specific energy consumption for an auger compactor for various densification treatments. The values are shown in Table 6 along with the ETLR. Using the values that Franz computed, the same container volume, and the same transportation energy input, the return on investment for corn stover is higher than miscanthus and means that corn stover can compete as well.

Table 6: Energy-to-Transportation/Loading Ratio for Corn Stover Using Values from Franz [21]

<b>Compaction Pressure (kPa)</b>	<b>Density (kg/m<sup>3</sup>)</b>	<b>Specific Energy Consumption (kJ/kg)</b>	<b>E<sub>src</sub> (kWh<sub>th</sub>)</b>	<b>E<sub>load</sub> (kWh)</b>	<b>ETLR</b>
15.28	170.92	17.69	512.67	0.52	125.67
20.37	171.83	15.43	515.40	0.45	128.33
24.25	214.77	21.51	644.19	0.79	148.04
38.66	248.64	23.61	745.79	1.00	163.38
63.06	297.5	29.35	892.34	1.49	176.62
116.08	342.59	35.17	1027.59	2.05	182.92



## CHAPTER 3

### MODIFIED SHIPPING CONTAINER

Sampling was proven to be a difficult task when testing the viability of shipping containers. Opening the container end caps allowed for sampling of the biomasses at each end. The bung holes at the top allowed for sampling at the top of the container, but samples were difficult to attain. A hay bale sampler probe, similar to the probe in Figure 17, was used for sampling [22]. The bale sampler probe is attached to a drill. The shaft has a serrated tip to cut into the bale, and the material travels through the shaft as it goes deeper into the bale. A cleanout rod pushes material through the cutout in the shaft inside the protective shield. The main drawback of this method is that the material clogged inside of the shaft and would not flow up the shaft. This meant that testable samples of the core of the biomass in the center of the containers were not able to be taken.



Figure 17: Hay bale sampler probe. a) Components of the bale sampler [22], b) Inside of protective shield with cutout of shaft.

A sampling method that was proposed was rock core sampling. This is a similar concept to hay bale sampling except for concrete, sediments, or rocks. A special drill is used to drill into the substance and retrieve a cylindrical sample called a core sample. The main drawback of this method is that the drills used are for rocks which are not a flowable material. Due to this, there is no way to know for certain if flowable material like biomass could be retrieved. Buying a rock core sampler is very expensive, shown in Figure 18, so testing this method was not attempted due to impracticality. This meant that sampling collection of biomasses could only be done on the outer edges at the bung holes or end caps, so valuable samples towards the center of the containers were not able to be analyzed.

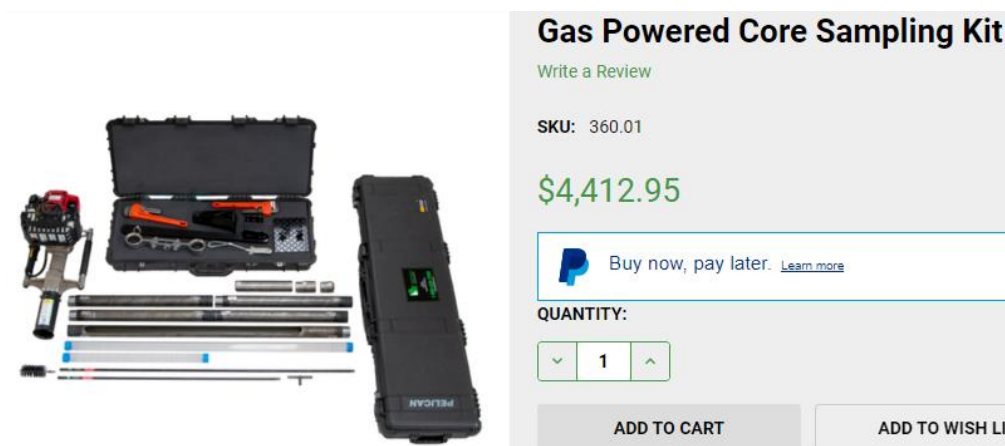


Figure 18: Gas powered core sampling kit from AMS, Inc [23].

### Modified Shipping Container Design

To overcome this sampling drawback, a modified shipping container is proposed. The modified container needs to allow for sampling towards the center of the container to be able to study the pre-treatment processes and determine the density of the biomass. The breakdown of the lignin of the biomass could be evaluated for chemical conversion and storage. Also, the

density could then be modeled as a function of depth in the container. The container model would only be used for sampling purposes.

The proposed design is a shipping container manufactured in three sections. The model is designed to be held together with hinges and clamps on both sides to replace the axial strength of the full-length container steel from the original container. The two end sections would have the ability to swing open after filling the container. The model should be strong enough to hold when filling and compressing the container with biomass. Two different models were developed using the student version of SOLIDWORKS 2020. The first model is based on the simplified design by Chip Energy used in the concurrent work, shown in Figure 19. The second model is modeled to resemble a standard 20 ft shipping container more closely, shown in Figure 23, that includes the transportation elements of fork pockets and lifting corners.

#### Modified Chip Energy Model

The original 5 ft container was built using 2-1/2" × 2-1/2" rectangular steel tubing as the structural frame of the container with two rectangular steel tubes acting as stands for the container at the bottom. The space between the two stands allows for movement of the container by forklift. Both longer sides of the container were corrugated steel walls. The roof has a corrugated design that is different to the sides and designed with bung holes to allow for sampling. The floor of the container was made of only steel unlike the typical wood 1" thick flooring of a standard container that is pressure treated to withstand saltwater exposure.

Figure 19 and Figure 20 display the modified container model based on the design by Chip Energy. Just like the original container, the rectangular tubing used for the structural frame was 2-1/2" × 2-1/2" rectangular low-carbon steel tube with 1/8" wall thickness from McMaster-

Carr. Unlike the original container, three independent tubes of 20" length were used at each side rail at the top and bottom on both sides of the container instead of one continuous tube. In between the top and bottom rails of each section where sections meet, 24" length tubes were placed to provide strength to the sections as well as a larger contact area between each section. On the top and bottom rails at the ends, rectangular tubes of 24" length were used while tubes of 29" length were used for the corner posts and the two stands at the bottom.

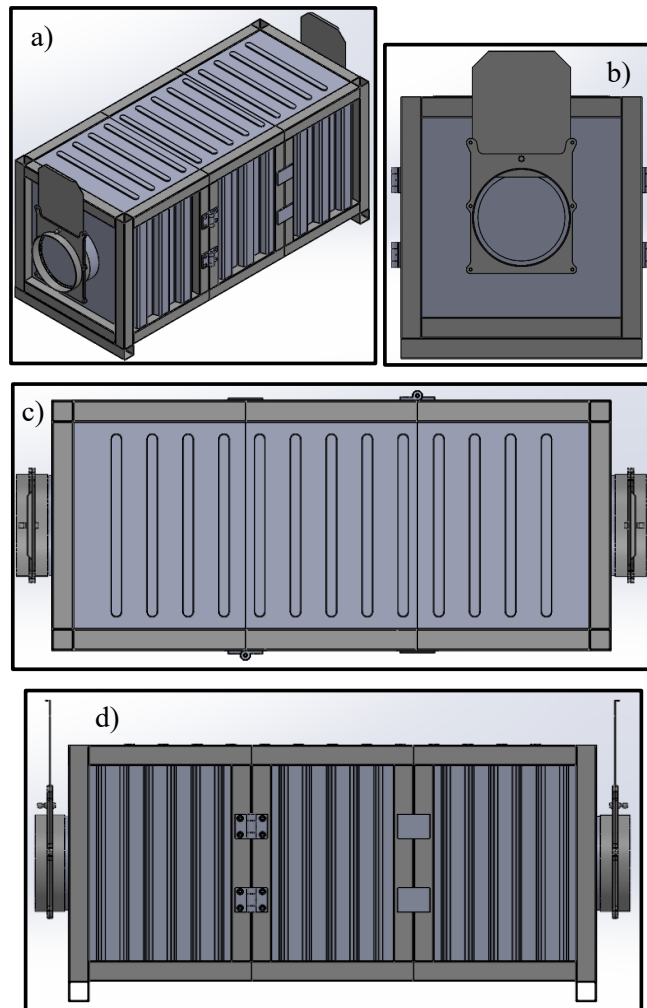


Figure 19: Modified Chip Energy container model. a) Isometric view, b) Front view, c) Top view, d) Side view.

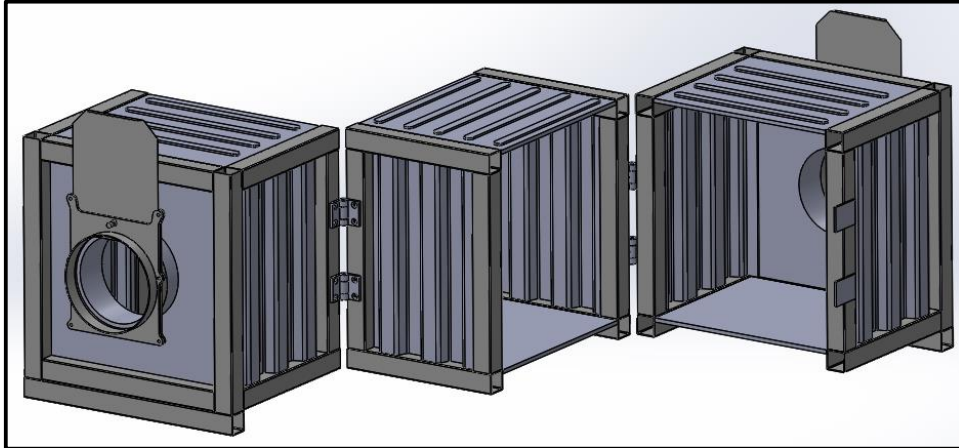


Figure 20: Modified Chip Energy container model with sections opened.

The floor was also split into three equal sections of 24" × 20" × 1/2" low-carbon steel. The roof has the same dimensions as the floor but has a corrugation profile on the top exterior, dimensions shown in Figure 21a. For the corrugated side walls, the height was 24" with both end sections having a width of 17.5" and the middle section having a width of 15". The dimensions for the corrugation profile of the side walls are shown in Figure 21b. Thickness for the side walls is 1/4". Every section is designed to have its components welded together.

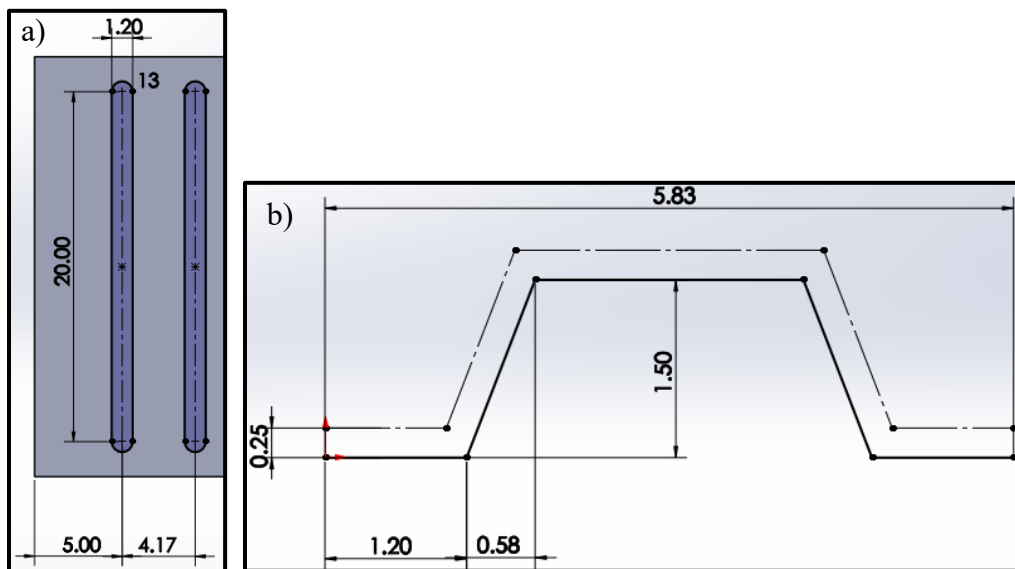


Figure 21: Corrugation profiles for the modified Chip Energy container. a) Roof, b) Side walls.

Similar to the actual Chip Energy container, each end wall has a hole with a diameter of 10.5" to allow for the auger to pass through when loading. An extrusion of 11.56" outer diameter and length of 4". The end wall has dimensions of 24"  $\times$  24"  $\times$  0.5". To allow for the end walls to be removed for biomass removal, plates were attached of 24"  $\times$  1.5"  $\times$  0.25" to the corner rectangular tubes. The end walls can be attached to these plates with screws. A sample blast gate from McMaster-Carr was added to close and open the auger hole, shown in Figure 22a.

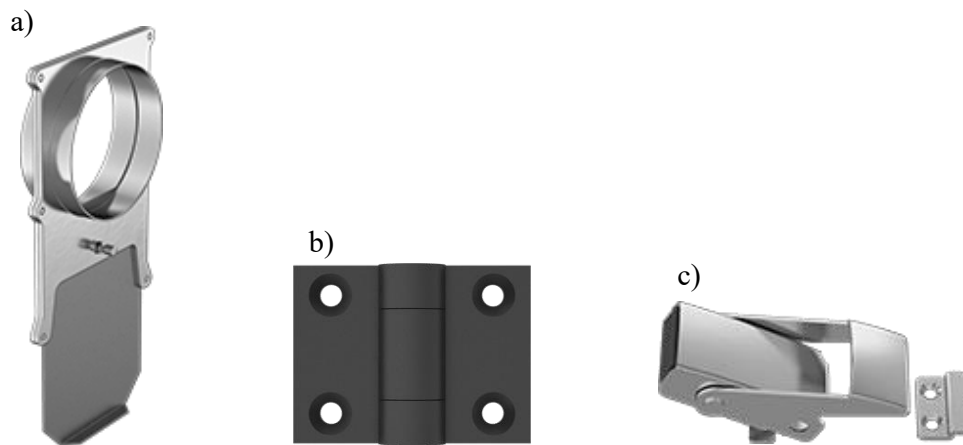


Figure 22: Parts used or suggested in the modified models from McMaster-Carr. a) Blast gate [24], b) Hinge [25], c) Latch [26].

The hinge used is displayed in Figure 22b and was heavy duty made of low-carbon steel from McMaster-Carr and has a load rating of 200 lbs. The dimensions are 3"  $\times$  2" door leaf and frame leaf for an overall width of 4" with a 0.375" leaf thickness. A latch is still to be determined, but one suggestion from McMaster-Carr is shown in Figure 22c. Two hinges and two latches were placed on both sides of the container. At the section contact regions where the latches should be, a plate was placed to be able to analyze the container with finite element analysis. The overall model dimensions are 65"  $\times$  29"  $\times$  31.63" with interior dimensions of about 60"  $\times$  24"  $\times$  26". This model can be used if a simple design is desired or necessary.

### Modified Standard Container Model

The model that resembles a standard 20 ft container is built similarly to the model based on the Chip Energy container. The same rectangular low-carbon steel tubing is used in this design as well as the same hinges and latch plates. The important differences between the two models are the corner posts and bottom rails. Both were designed to resemble their respective standard container components. This meant that dimensions for some components were different. For example, the roof and floor kept the same thickness, but dimensions changed to accommodate corner posts.

The modified standard container model is displayed in Figure 23, Figure 24, and Figure 25. Changing rectangular tubes for corner posts similar to standard container posts caused the model to have different overall dimensions and required some of the design to be changed from the Chip Energy model. The corner posts had a height of 24", and their profile is shown in Figure 26. This caused the top side rails to stop being in line with the top end rails, so corner blocks were added. These blocks emulate the corner fittings of standard container. The blocks are 3.75" × 3.75" × 2.5".

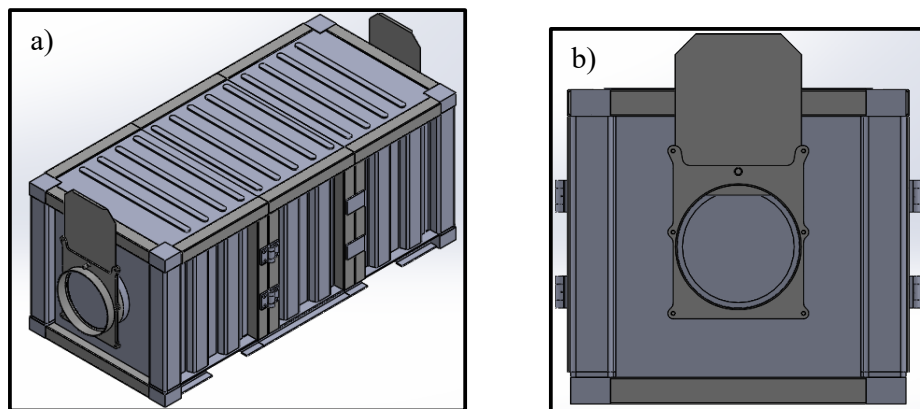


Figure 23: Modified standard container model with two views. a) Isometric, b) Front.

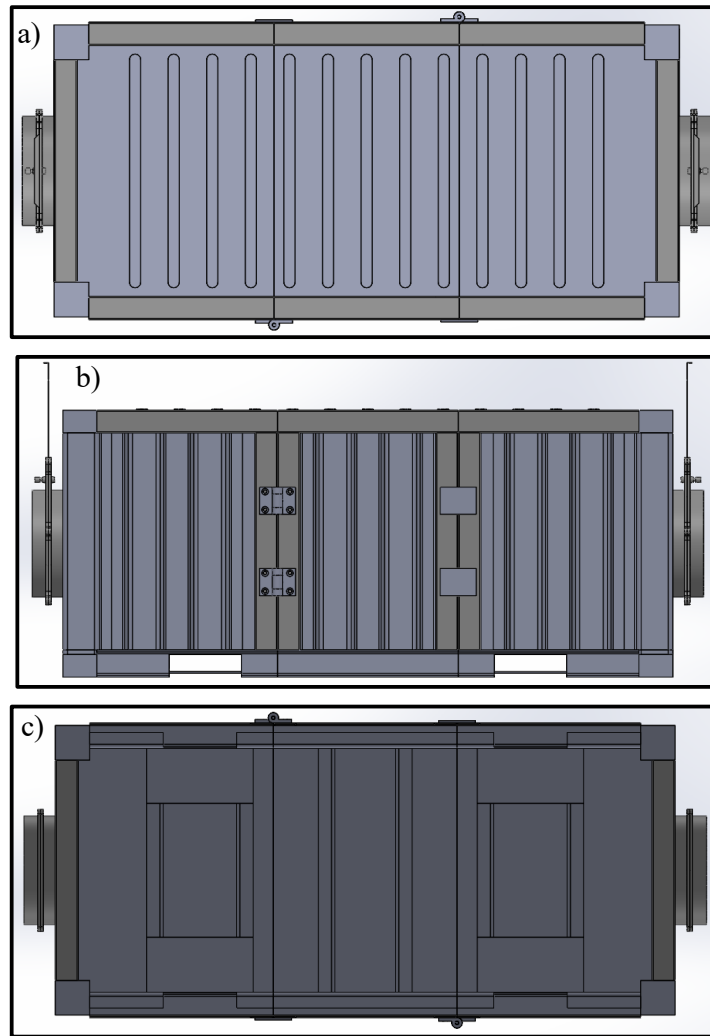


Figure 24: Modified standard container model with different views. a) Top, b) Side, c) Bottom.

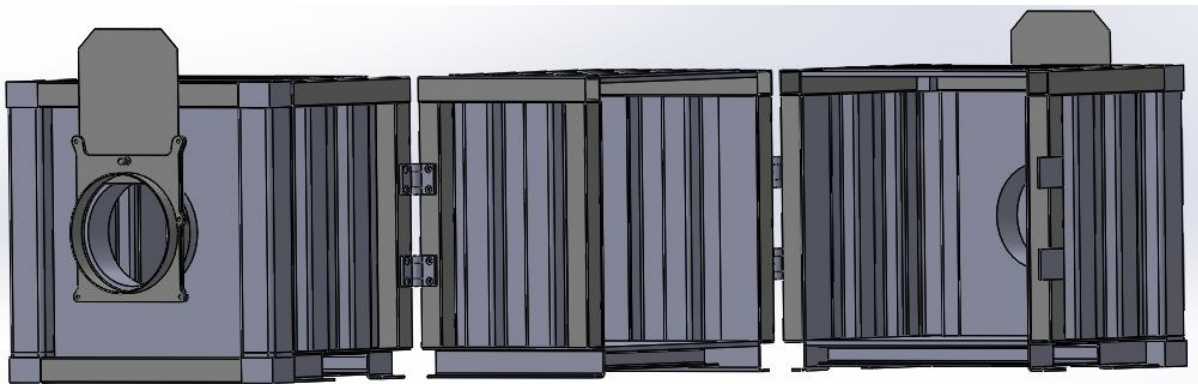


Figure 25: Modified standard container model with sections opened.



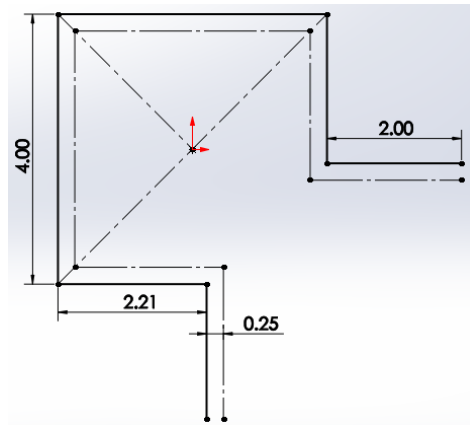


Figure 26: Corner posts profile for the modified standard container.

Plates of  $24'' \times 4.5'' \times 0.25''$  were added to the interior of the container at the rectangular tubes in the section contact regions to be in line with the corner posts on the sides of the container. The corrugated side walls are attached to the exterior of the plates as shown in Figure 27. Just like the modified Chip Energy model, the end walls had an auger hole with the same dimensions as well as the same blast gate. Instead of adding plates to screw the end wall onto, the corner posts already have a region that the wall can be screwed onto, shown in Figure 28. The overall end wall dimensions are  $24.5'' \times 23'' \times 0.5''$  with the extrusion having a 3'' length.

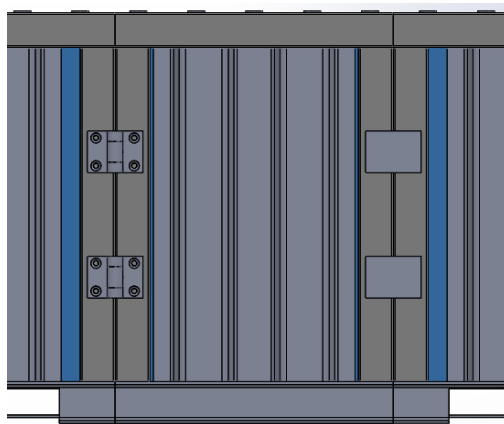


Figure 27: Side view of the modified shipping container that shows the placement of the side walls and tube plates (in blue).

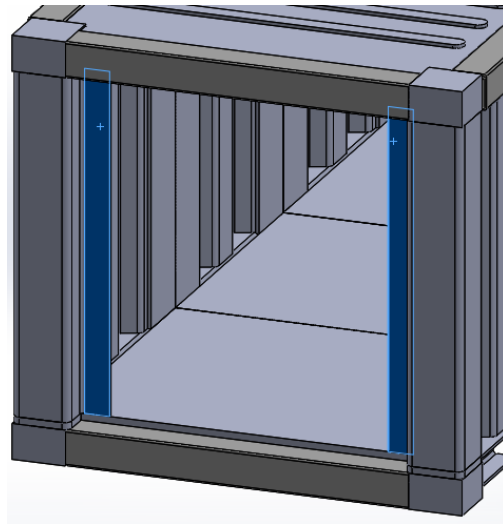


Figure 28: Corner posts region where the end wall is attached.

Adding corner posts caused the corrugated walls to be wider. For the corrugated side walls, the height was 24" with every container section having the same width of 14.5". The dimensions for the corrugation profile of the side walls are shown in Figure 29. The same top and bottom rails around the container were kept the same as the modified Chip Energy model. The floor has dimensions of 26.58"  $\times$  21.54" for the end sections, and the middle section has the same length, but a width of 20". Plates were added at the bottom of the corner posts to be able to cover that region so that material did not exit through that region and placed the bottom corner blocks in line with the bottom rails. The dimensions are the same as the corner posts profile with the same thickness as the floor for consistency. The roof has the same corrugation profile as shown in Figure 21a but 4" longer as the dimensions of the roof are now 27.08"  $\times$  21.25" for the end sections. The middle section has a roof width of 20". To accommodate the corner blocks, two corners of the roof for the end sections have cuts of 1.54"  $\times$  1.25".

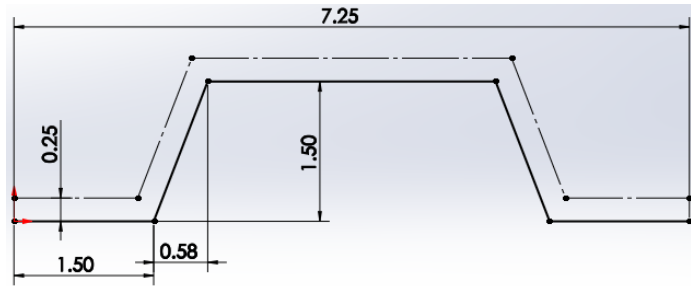


Figure 29: Corrugation profile of the side walls for the modified Chip Energy container.

The bottom rails were c-beams instead of rectangular tubes to resemble a standard container. Since the container needs to be able to be lifted by forklifts, each end section bottom rail had a cut out to allow for forks to pass through, shown in Figure 24b. Each bottom rail had a length of 20" and the profile demonstrated in Figure 30a. Cross members, with the profile in Figure 30b, were added underneath the floor that stretched from the bottom rail on one side of the container to the other. Two cross members were attached at bottom rail cutouts for each end section to add stability to the bottom rails as well as two for the middle section. A 7-gage thick fork plate was also added to the end sections at each bottom rail cutout underneath the cross members of 11.6" × 6" to have a forklift pocket. Every section is designed to have its components welded together just as the previous model. The overall model dimensions are 67.5" × 31.5" × 29.63" with interior dimensions of about 60" × 24" × 26". This model can be utilized if a more complex model that resembles a standard shipping container is desired or needed.

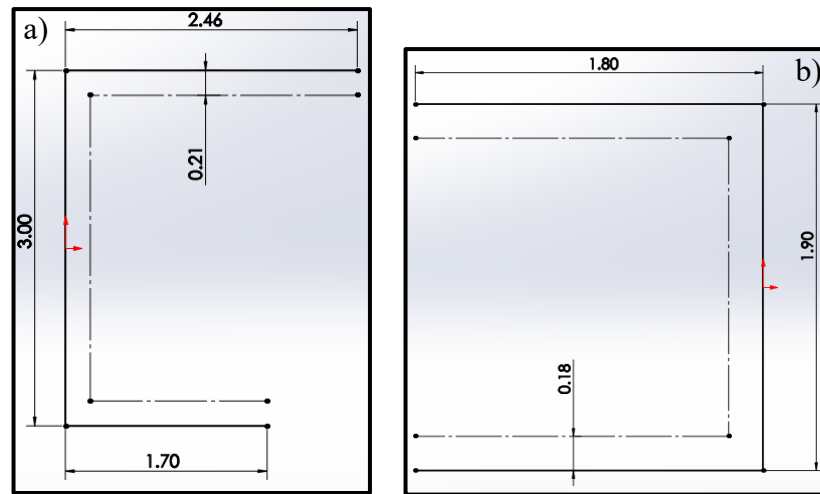


Figure 30: Profiles for the modified standard container. a) Bottom rails, b) Cross members.

### Finite Element Analysis

A finite element analysis was done on both models to determine whether the containers can withstand the pressure of the loaded biomass. The student version of ANSYS Workbench 2019 R2 was used for analysis with a static structural simulation. The stress and deformation were studied to determine the durability of the models from the pressure after loading. Since all the components from McMaster-Carr of both models were made of low-carbon steel, the material used in ANSYS was the default material: structural steel. The reason to use this material is that low-carbon steel has similar properties to structural steel due to structural steel being a general material that includes carbon steel. Properties of structural steel are shown in Figure 31. The important aspect of the design will be whether the seams open; hence the elastic modulus is important to the characterization of loading the 3-piece containers.




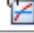
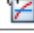

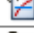
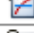

 Density	490.06	lb ft <sup>-3</sup>
 Isotropic Secant Coefficient of Thermal Expansion		
 Isotropic Elasticity		
 Strain-Life Parameters		
 S-N Curve	 Tabular	
 Tensile Yield Strength	36259	psi
 Compressive Yield Strength	36259	psi
 Tensile Ultimate Strength	66717	psi

Figure 31: Properties of the structural steel material from ANSYS.

The constraints of the models are simple. Fixed supports were added to the bottom end rail for the modified standard container and to the bottom end stand for the modified Chip Energy container of one end section of the models, displayed in Figure 32. Because the model rests on the floor and is connected to an auger on one of the end sections, the fixed supports were added to those ends only. Frictionless supports were added to the other components that touch the ground. This should allow for displacement of the other sections which will lead to a displacement study. Stress on the hinges can then be determined as well. The meshes for the models are shown in Figure 33 and had the default element size except for the hinge components which had an element size of 1 in for the modified Chip Energy container and 0.5 in for the modified standard container. This was due to stress singularities appearing on the hinge components with a larger element size. The elements of the meshes have a

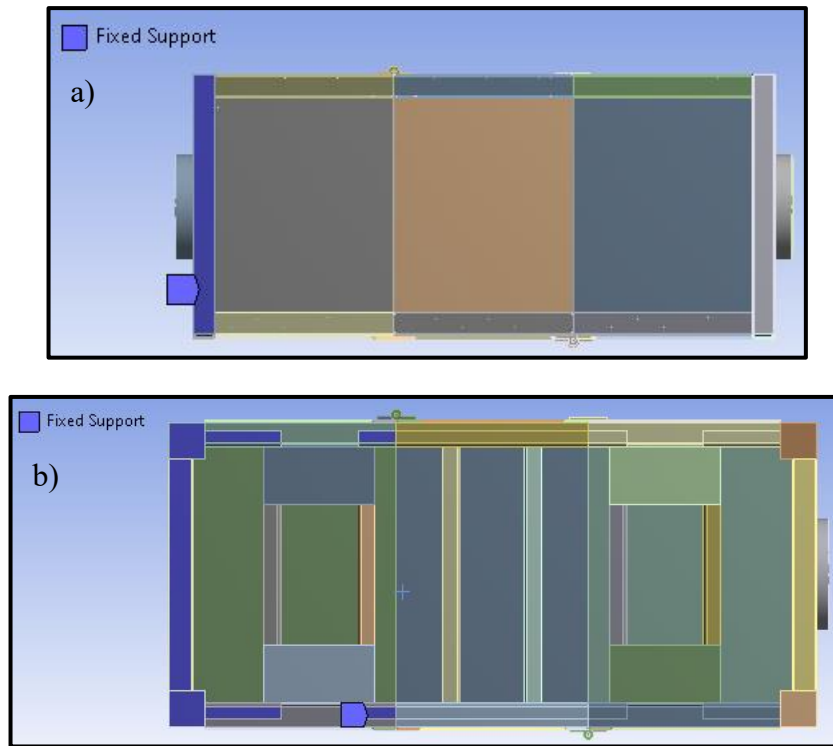


Figure 32: Fixed supports for the containers in ANSYS. a) Modified Chip Energy model, b) Modified standard container model.

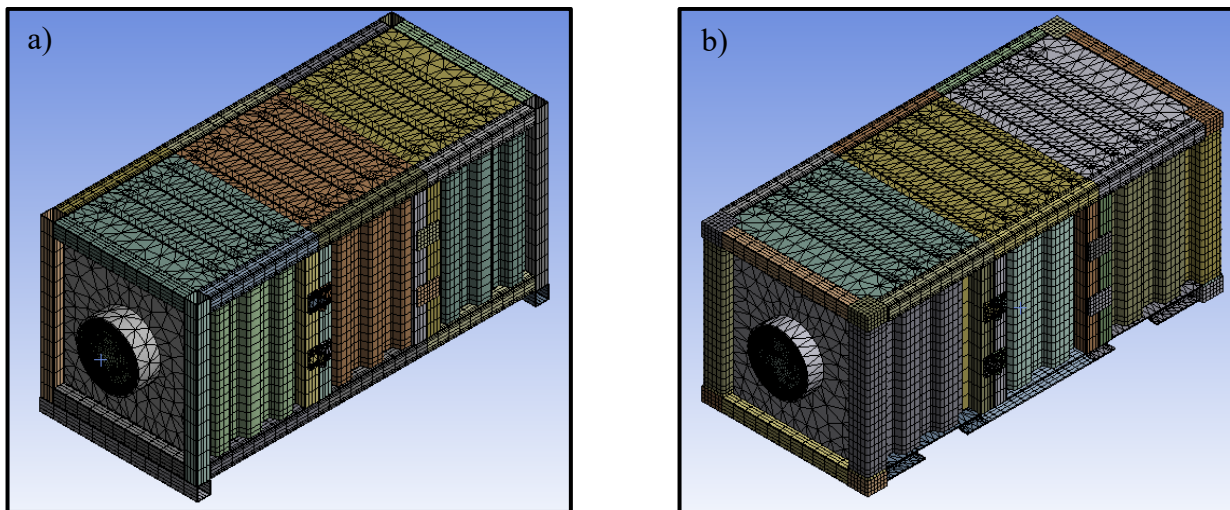


Figure 33: Mesh used for the containers in ANSYS. a) Modified Chip Energy model, b) Modified standard container model.

Since most of the container model parts are welded together, this means that most of the contacts will be bonded. This does not allow the components to slide against each other or separate from each other. The end walls are bonded to components that they will be connected to with screws. Components that need to move will have the contact type of no separation. This allows for sliding against each other but no separation between the components. Both contact types are linear and allow for a quick and simple analysis. Attempts were made to use nonlinear contact types between the faces of the three sections with holding forces from the hinges and latch, but the student version did not allow for solving of the analysis due to the nonlinearity of the contacts. To simulate the blast gate slide, a plate of similar thickness to the suggested blast gate slider was added. The slide plate had a bonded contact with the end wall extrusion.

A pressure distribution from the biomass compaction was applied to the interior walls of both models. The pressure was calculated using an equation based on the Janssen pressure [27] for vertical silos, shown in Figure 34. This pressure is generated from the gravitational force acting on the material in the silos. Parts of the Janssen pressure equation had to be modified to accommodate the horizontal nature of the loading and containers as well as the pressure generated from compacting the biomass with an auger.

$$p_h = p_o \left[ 1 - e^{-z/z_o} \right] \quad (1)$$

in which  $z$  is the depth below the equivalent surface,  $\gamma$  is the stored solid unit weight and  $p_o$  is the asymptotic pressure at great depth given by

$$p_o = \frac{\gamma A}{\mu U} \quad (2)$$

and the characterising depth  $z_o$  is given by

$$z_o = \frac{1}{K\mu} \frac{A}{U} \quad (3)$$

where the wall perimeter is  $U$ , the plan cross-sectional area is  $A$ , the wall friction coefficient is  $\mu$  and the mean lateral pressure ratio is  $K$ . The hydraulic radius is given by  $A/U$ .

Figure 34: Janssen pressure equations indicating the decaying exponential form [27].

The general Janssen equation was kept the same to have a maximum pressure that decayed only in a region of the container. The depth into the container is now horizontal instead of vertical for the silos with the equivalent surface being the interior of one of the end walls of containers. Since the driving force for the pressure acting on the containers is the force from the auger, instead of using the asymptotic pressure equation from Goodey et. al., the asymptotic pressure is calculated with equation (5). The force from the auger is  $F$ , the wall friction coefficient is  $\mu$ , the cross-sectional area is  $A$ , and the cross-sectional perimeter is  $U$ .

$$p_0 = \frac{F}{\mu A U} \times \frac{A}{U} = \frac{F}{\mu U^2} \quad (5)$$

The force acts on the cross section of the container with the perimeter being the distance being acted on at that point of the container. The squared perimeter drives the maximum pressure which practically the square of the total area. This replaces the specific weight in the original asymptotic pressure equation. The equation for the characterizing depth stays the same.  $K$  is the ratio between the horizontal stress and vertical stress. Crawford et. al. found that  $K$  is about 4.17 and the wall friction coefficient is about 0.18, but was rounded up to 0.2 for this analysis, for miscanthus using a normal load of 15 kPa (2.18 psi) [28].

To determine the force from the auger, the loading energy data of the miscanthus was used from the concurrent work. The auger ran until it stopped jamming biomass in the container and began “stalling”. This meant that the auger ran until it finished filling the container and began to compact the miscanthus. The region of the loading data that compacted the miscanthus was used to determine the compacting pressure on the biomass and therefore the containers. This region was where the current began spike until the motor was turned off, shown in Figure 12. The compaction energy was found using equation (2), and the total was 137,628.89 W\*sec.



Then, the energy was divided by the time region (76.8 – 101.6 sec) of the “jamming” to get the power of the motor. The motor’s rated rpm is 1725 shown in Figure 10. Assuming the jamming of the biomass was occurring at 40% of the motor’s rated rpm, the angular speed of the motor was 690 rpm. Figure 35 displays the equation that is used to determine the auger rpm which helps to find the torque of the auger. The auger had both the drive and driven pulleys of 3.5” diameter and a gearbox reduction ratio of 25.64 to 1. The auger had a speed of 26.91 rpm.



Figure 35: Equations to calculate the rpm of an auger [29].

The torque of the auger can be calculated with equation (6), with a resultant torque of 1969.24 N\*m. The diameter of the auger flighting was 9” and the auger shaft had a 2” diameter. The acting arm of the force is the difference between the flighting and shaft divided by two at a 90° angle. This torque is then used in equation (7) to finally calculate the force from the auger. The force of the auger was calculated to be 4980.03 lbs. Plugging the force into equation (5) and using the equations in Figure 34 calculates the pressure distributions for the models shown in Figure 36 and Figure 37. Both distributions are comparable to the normal load of Crawford et. al. and the smallest compaction pressure from Franz shown in Table 6. The asymptotic pressures were similar to the normal load utilized by Crawford et. al. [28] and the minimum compaction pressure from Franz [21]. The power is  $P$ , the revolutions per minute is  $n$ , the flighting radius is  $r_f$ , the shaft radius is  $r_{sh}$ , and the angle between the force and moment arm is  $\theta$ . The pressures were imported into ANSYS to find the deformation and stress of the containers.

$$T = \frac{P}{2\pi (n/60)} \quad (6)$$

$$F = \frac{T}{(r_{fl} - r_{sh})\sin\theta} \quad (7)$$

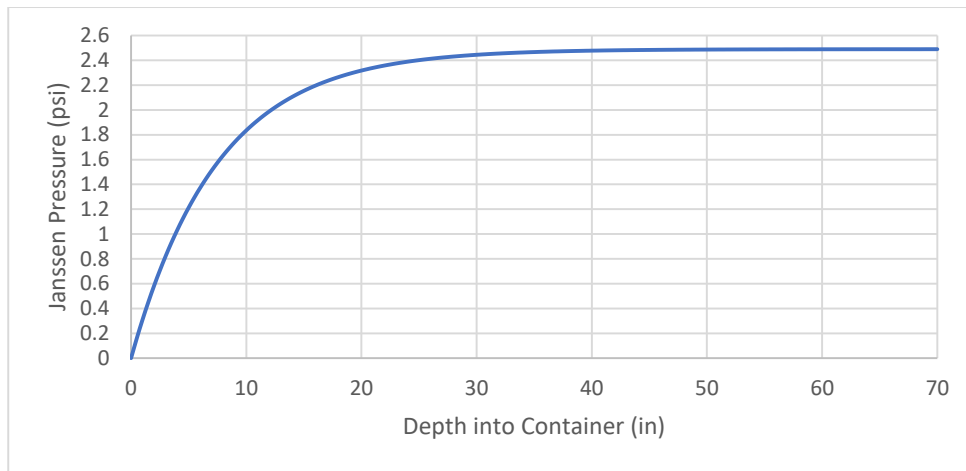


Figure 36: Pressure distribution for the modified Chip Energy model.

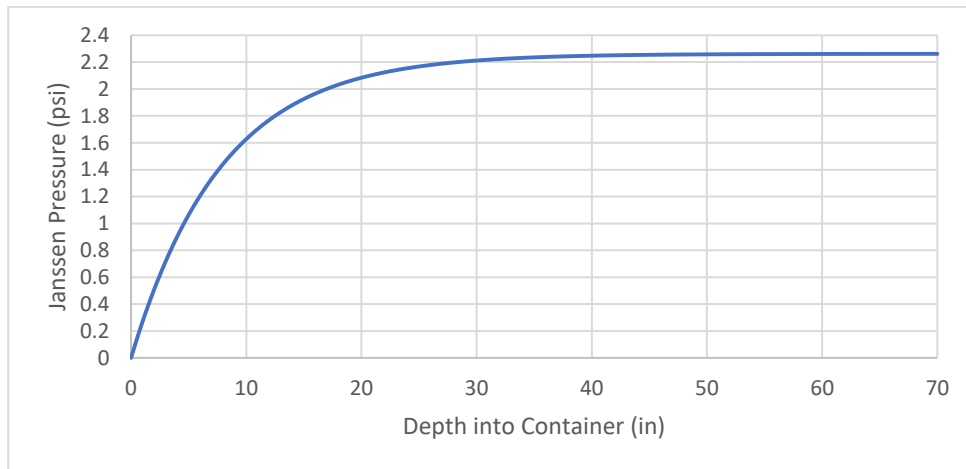


Figure 37: Pressure distribution for the modified standard container model.

Figure 38 shows the blast gate slider emulator plate analysis results of the modified Chip Energy container. The deformation in the z-direction was about 0.115" which seems slightly high for a plate that is 0.05" thick, but the equivalent stress was about 25708 psi which is lower than the yield strength of the material shown in Figure 31. The actual blast gate structure will give the

slider more strength, but the blast gate can be replaced with a blast gate with a thicker slider if the slider deforms when tested.

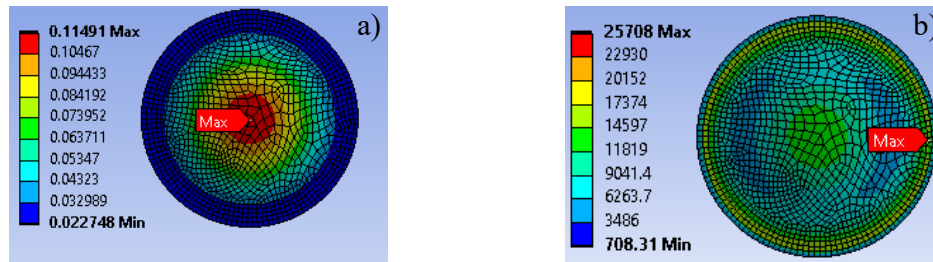


Figure 38: ANSYS results for blast gate slider of the modified Chip Energy model. a)

Deformation in the z-direction, b) Equivalent stress of blast gate.

Figure 39 shows the equivalent stress on the modified Chip Energy container. The max stress, at the hinges, is about 35013 psi which is lower than the yield strength of the material shown in Figure 31. This stress is very close though, so a stronger hinge might be necessary or maybe cross members underneath the floor to help sustain the container floor from bending. The problem with this stress is that it seems to be a stress singularity. Instead of the maximum stress being on the pin, the stress only appears on one fillet of the leaf. The rest of the container has a very small stress, so the design seems to hold well after loading.

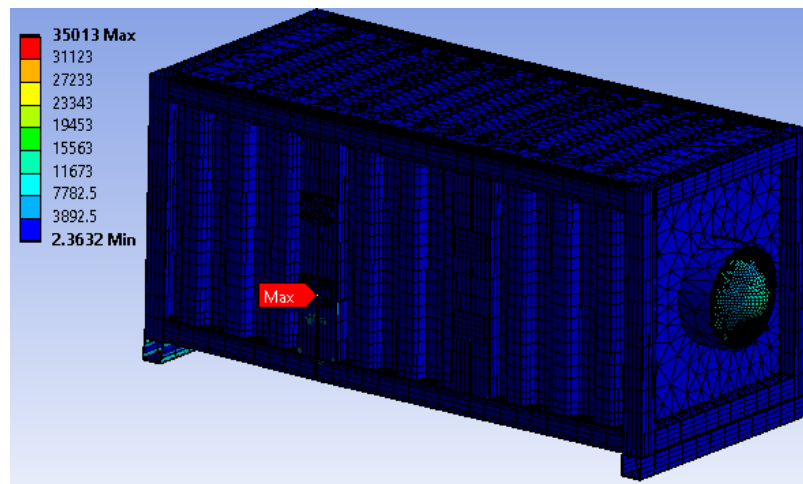


Figure 39: Equivalent stress on the modified Chip Energy container.

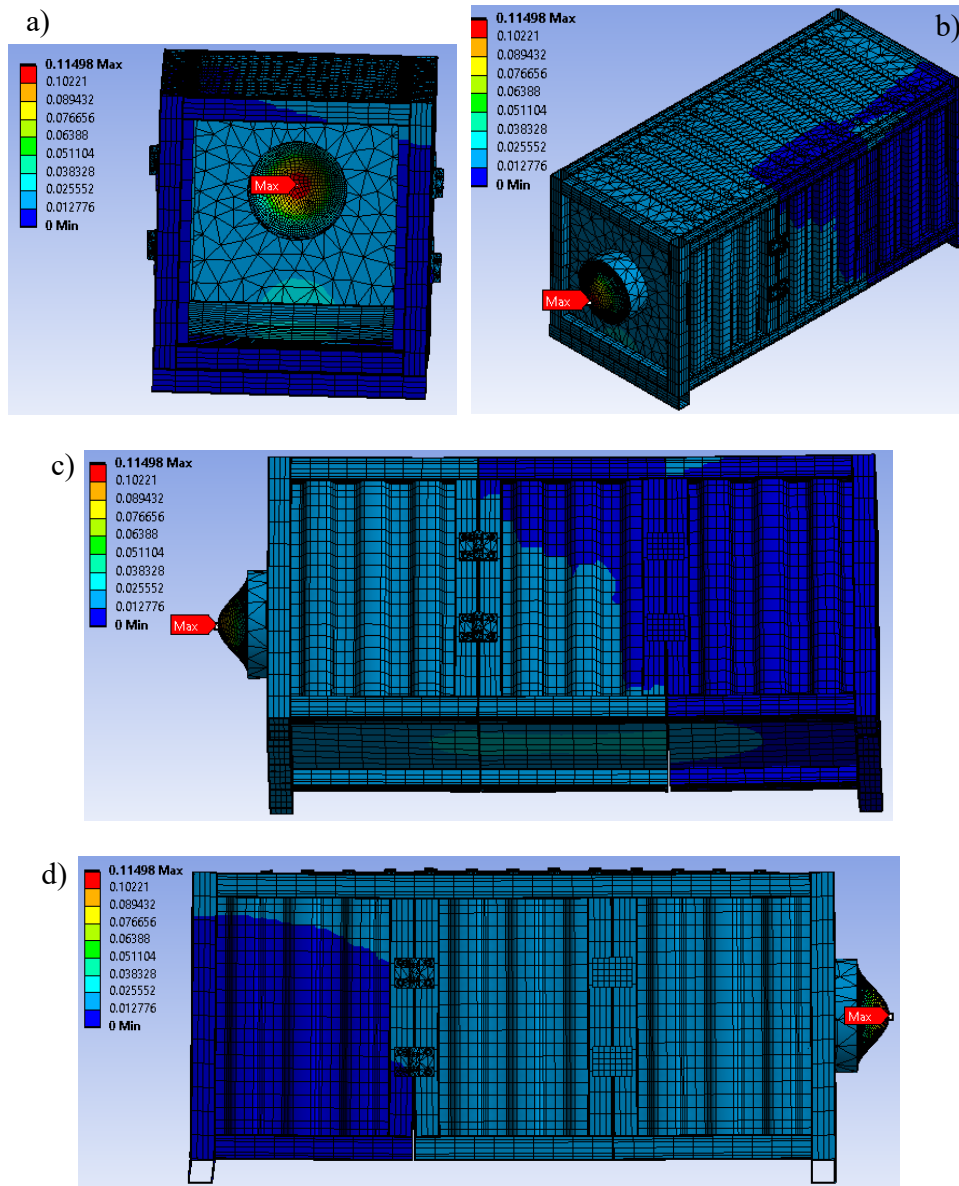


Figure 40: Deformation results of the modified Chip Energy container. a) Front view, b) Isometric view, c) Left side view, d) Right side view.

The deformation of the entire modified Chip Energy container is shown in Figure 40. The highest deformation is the slider of the blast gate with the rest of the container having a smaller deformation. The container has a deformation in between 0.02” and 0.03” which is not high. The biomass is unlikely to fall out of the container after loading.

Figure 41 shows the blast gate slider emulator plate analysis of the modified standard container. The deformation in the z-direction was about 0.096” which seems slightly high like the other container model and the equivalent stress was about 22626 psi. Both results are lower than the modified Chip Energy container.

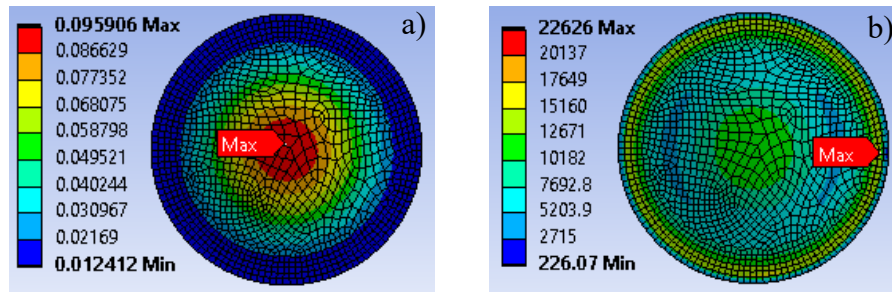


Figure 41: ANSYS results for blast gate slider of the modified standard container model. a) Deformation in the z-direction, b) Equivalent stress of blast gate.

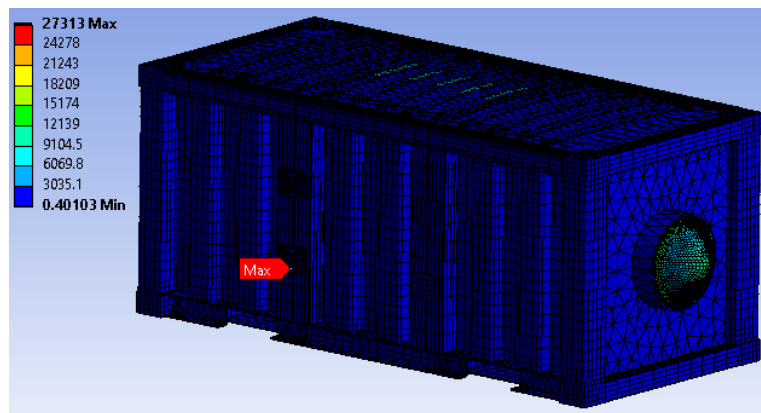


Figure 42: Equivalent stress on the modified standard container.

The equivalent stress of the modified standard container is shown in Figure 42. There is a stress difference of about 8 psi between the two containers, but the modified standard container equivalent stress is still under the yield strength. Just as the modified Chip Energy container, the highest equivalent stress was at the hinges. The deformation of the entire modified standard container is shown in Figure 43. The container has a deformation in between 0.01” and 0.02”

which is lower than the deformation of the modified Chip Energy container. The biomass is unlikely to fall out of the container after loading. It seems that the cross members and corner posts added to the strength of the container. Another reason for the lower results is the cross-sectional area of the modified standard container. The larger cross-sectional area and perimeter results in a lower pressure curve that reduces the stress and deformation of the container.

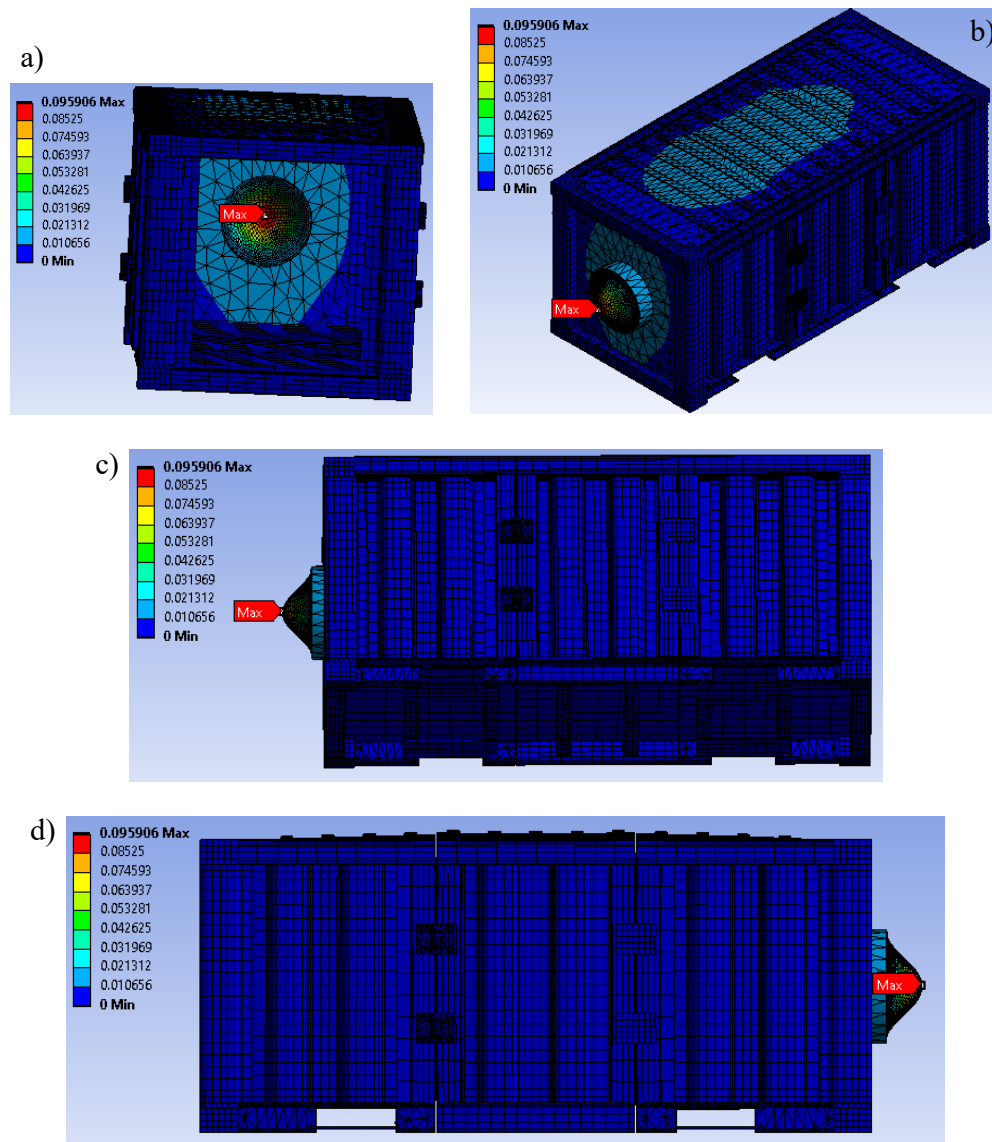


Figure 43: Deformation results of the modified standard container. a) Front view, b) Isometric view, c) Left side view, d) Right side view.

### 3D Printed Scaled Containers

One-eighth scaled containers were 3D printed using a Creality Ender 3 for demonstration of the containers and to test the viability of the hinge container design. Figure 44 and Figure 45 show the scaled Chip Energy container model. The scaled modified standard container model is shown in Figure 46 and Figure 48. The filament used was 1.75 mm diameter PLA and 100% infill was used. Both models were scaled in SOLIDWORKS and modified where needed. The section assemblies were turned into STLs for each section and printed separately. Ultimaker Cura was used to slice the STLs to output G-code. Since the containers were scaled, different hinges and latches were used. Figure 49 shows the hinge and latch parts from McMaster-Carr that were used. The rectangular tubes were turned into bars by filling the inside of each to allow for easier printing, a stronger model, and for screws to be attached. The scaled containers were modified to be able to secure the latches in place and to add a 3D printed blast gate.



Figure 44: Scaled modified Chip Energy model front view with blast gate off.





Figure 45: Scaled modified Chip Energy model. a) Top view, b) Side view, c) Opened container top view, d) Opened container side view.



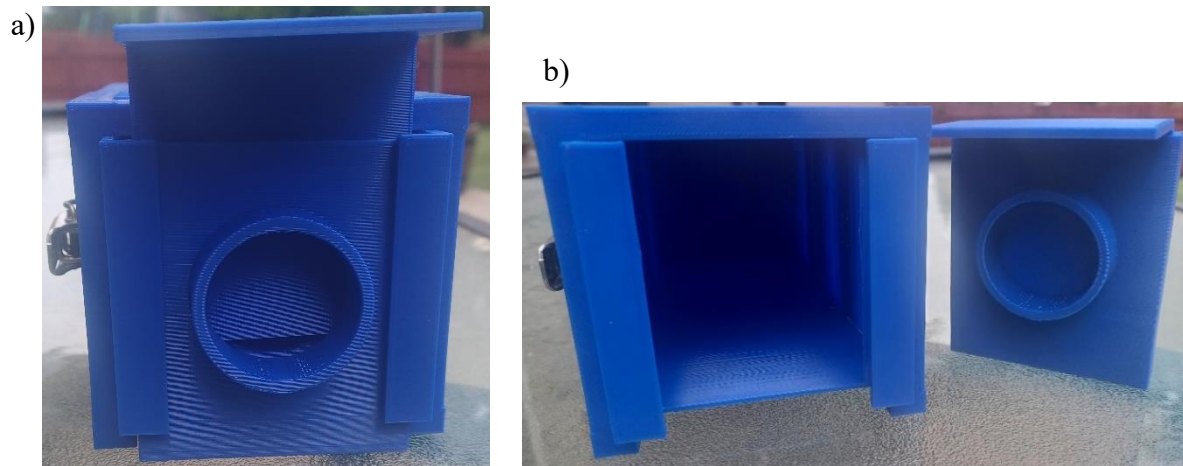


Figure 46: Scaled modified standard container model. a) Front view, b) Blast gate off view.



Figure 47: Scaled modified standard container model. a) Top view, b) Bottom view.



Figure 48: Scaled modified standard container model. a) Side view, b) Opened container view.



Figure 49: Parts used for the scaled models from McMaster-Carr. a) Hinge [30], b) Latch [31].

For the latches, Figure 50 shows the placement of one of the latches on the scaled standard container model. The side wall had extrusions added to the exterior and interior to extend the area of contact between the latch and side wall on both sides of the container. This allows for the latch to be lined up with the strike plate that is attached to the rectangular tubes. The scaled Chip Energy container also had similar extrusions on the side walls. Also, the extrusion gives more thickness to the side wall to hold the screw.

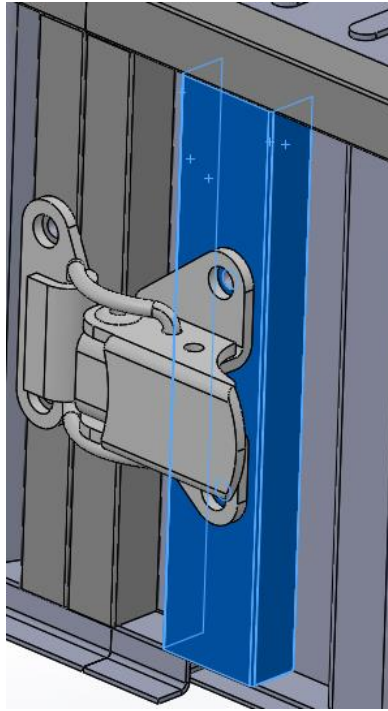


Figure 50: Extrusion added to the side wall of the scaled standard container model for the latch.

Extrusions were also added to the corner posts and corner tubes to hold a blast gate. These extrusions are displayed in Figure 51. The blast gates that are connected to the models on both end sections. The blast gate for the scaled Chip Energy model was designed to cover the entirety of the area where the end wall would be placed. For the scaled standard container model, the blast gate was designed to fit underneath the top end rail and between the corner posts. The 1.5” diameter holes in the blast gates allow for a handheld drill auger to pass through to fill the containers. The printed blast gates were made to slide into the region between the extrusions and the containers as a friction fit.

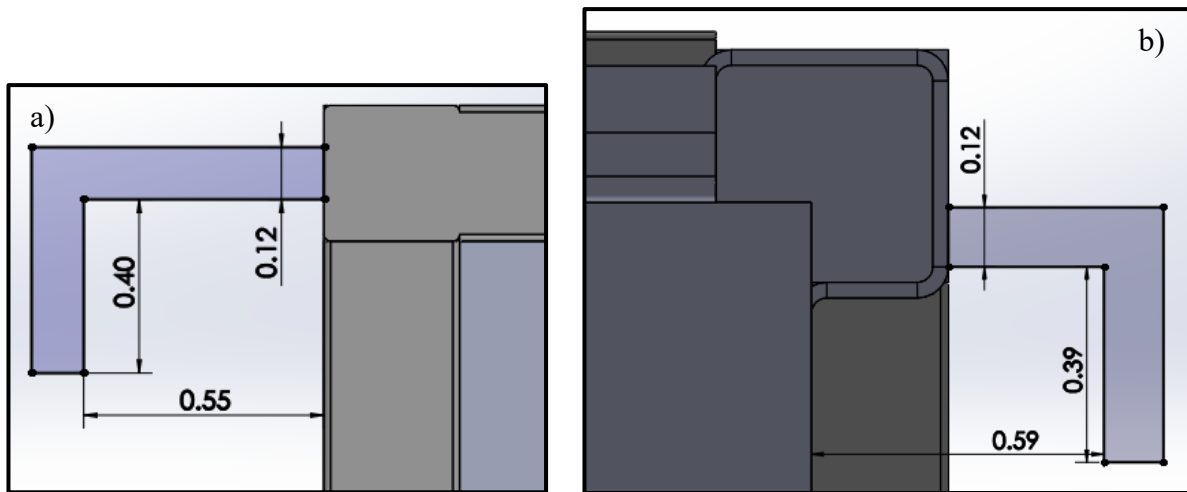


Figure 51: Extrusion profile for the scaled containers. a) Chip Energy model (top view), b) Standard container model (bottom view).

The printed container models had a few inconsistencies. Some of the support material was difficult to remove. This caused some of the support material to stick to the model and not able to be completely removed. Another inconsistency was the thickness of some of the thinner components. These components were not able to be printed with much thickness and thus tended to break. Fortunately, those components are not highly important to the model. Since each section was printed separately, the sections tended to warp slightly and caused the sections to not be completely flush to each other. The sections still held together tightly and with no major gaps. These 3D printed models will lead to future bench-top testing of the hinge design.

## CHAPTER 4

### CONCLUSION

This thesis was intended to help determine the viability of using shipping containers to transport biomass. The first component was determining the energy return on investment (energy-to-transportation and loading ratio in this thesis) of miscanthus and corn stover compared to coal and natural gas. Using the volume of the container in the concurrent work, the total energy for each source was calculated alongside the energy consumption of the loading process and transportation respectively. The energy-to-transportation and loading ratio is the ratio of energy output and energy input. Coal had an ETLR of 269, and natural gas had an ETLR of 51. For the biomasses, miscanthus had an ETLR of 103, and corn stover had an ETLR of 31. Even though the biomasses have low ETLR compared to coal, the benefit to using biomass is the ability to improve the density in the containers. This is shown by Franz in Table 6. As the density of corn stover increases, the ETLR increases as well. This results in corn stover reaching an ETLR level of about 183 for a density of about 343 kg/m<sup>3</sup>. Miscanthus has the possibility to achieve higher ETLR as well if the density increases. Higher transportation distances, especially for truck transportation, will lower the ETLR. This component of the thesis was able to show that biomass can compete as an alternative with prevailing fossil fuels in terms of energy investment returns using shipping containers.

The other component of the thesis was creating two ¼-length scaled modified shipping container models to allow for easier sampling for the concurrent work. This component will help

the concurrent work to determine which pre-processing treatments allow for lignin breakdown and what the local density is towards the center of the container. One of the models was based on the concurrent work container and the other was based on a standard 20 ft shipping container. The models were each divided into three sections and held together with hinges and clamps. The end walls were designed to allow an auger to pass through to fill with biomass and be closed with a blast gate. Finite element analysis was done on both containers to determine the viability of the hinge design. The deformation and stress for both containers were low, so the hinge design can be utilized. For most of the models, the stress is significantly lower than the yield strength of the material. The issue was the blast gate and hinges suggested, but those can be easily replaced. 1/8-length scaled models were 3D printed for demonstration and prototype testing. Both components of the thesis were shown to further biomass as an important sustainable energy resource.

### Future Work

A few factors are needed in the future to further along the work done in this thesis. A proper removal process from the containers is needed. Upon compaction inside a shipping container, the biomass will have a nearly solid, brick-like shape. Due to the interior corrugation of the container, removal will require some subsequent design that requires minimal energy inputs. In the proposed model, the end walls are designed to be removed which allows for the possibility of using a tip truck to dump the biomass out of the containers. Whether the densified biomass will naturally fall from the container will need to be tested. Furthermore, downstream conversion processes will need to separate the material for flowability in whatever system is used for biofuels, special chemicals, or other products from the biomass.

Another factor is calculating overall energy consumption of the biomasses. Chapter 3 was a more simplified calculation to demonstrate the viability of biomass and shipping containers. This meant that the energy consumed to harvest the fields, the energy consumed by workers, the energy consumed by every piece of machinery, etc. was not included in the calculation. Life cycle assessments are part of all requests from Department of Energy technical proposals. Looking narrowly at a process can result in claims such as electric cars having zero emissions. However, the full life cycle would consider from the original sunlight storage source to the end use. In the same way fossil fuel consumption should start from first extraction from the Earth, the full return on investment in biomass would need to start from planting seeds and include all landscape maintenance and collection. Future systematic studies will continue to shed light on the viability of biomass as an authentic renewable resource.

Finally, the final factor needed is a design review. Due to time constraints of the completed design and availability of graduate students during a summer term, a peer design review was not able to take place. Reviews for both model designs are needed before moving to manufacturing the containers. Feedback gained from the review of specifications to the subsequent performance analysis would aid in fabrication and operational elements. When the final design review is completed, NIU looks forward to partnering with Chip Energy to implement full-scale features for testing, proof of concept, and hopefully operations.

## REFERENCES

- [1] “Biomass Explained - U.S. Energy Information Administration (EIA)” [Online]. Available: <https://www.eia.gov/energyexplained/biomass/>. [Accessed: 06-Jun-2023].
- [2] “Energy Density - Energy Education” [Online]. Available: [https://energyeducation.ca/encyclopedia/Energy\\_density](https://energyeducation.ca/encyclopedia/Energy_density). [Accessed: 31-Mar-2023].
- [3] Lizotte, P.-L., Savoie, P., and De Champlain, A., 2015, “Ash Content and Calorific Energy of Corn Stover Components in Eastern Canada,” *Energies*, **8**(6), pp. 4827–4838.
- [4] Gushchina, V. A., Volodkin, A. A., Ostroborodova, N. I., and Lykova, A. S., 2022, “Miscanthus Giganteus in the Middle Volga Region: Opportunities and Prospects,” *IOP Conf. Ser. Earth Environ. Sci.*, **953**(1), p. 012008.
- [5] “Ethanol Explained - U.S. Energy Information Administration (EIA)” [Online]. Available: <https://www.eia.gov/energyexplained/biofuels/ethanol.php>. [Accessed: 06-Jun-2023].
- [6] Connection, K. F. F., 2016, “Fun Facts About Corn Harvest,” *Kans. Farm Food Connect.* [Online]. Available: <https://kansasfarmfoodconnection.org/spotlights/fun-facts-about-corn-harvest>. [Accessed: 06-Jun-2023].
- [7] pnmralex, “Soybeans Plants Seeds - Free Photo on Pixabay” [Online]. Available: <https://pixabay.com/photos/soybeans-plants-seeds-bag-burlap-2039642/>. [Accessed: 06-Jun-2023].
- [8] “Biofuels Explained - U.S. Energy Information Administration (EIA)” [Online]. Available: <https://www.eia.gov/energyexplained/biofuels/>. [Accessed: 06-Jun-2023].
- [9] Crane, M., 2012, “Harvesting Miscanthus in Southern Kentucky,” *Dubois Cty. Free Press Inc* [Online]. Available: <https://www.duboiscountyfreepress.com/harvesting-miscanthus-in-southern-kentucky/>. [Accessed: 06-Jun-2023].
- [10] Eise, J., “Purdue Study Shows Potential for Growth in Biofuels from Corn Stover - Purdue University” [Online]. Available: <https://www.purdue.edu/newsroom/releases/2015/Q4/purdue-study-shows-potential-for-growth-in-biofuels-from-corn-stover.html>. [Accessed: 06-Jun-2023].
- [11] Mitchell, R., and Schmer, M., 2012, “Switchgrass Harvest and Storage,” *Switchgrass*, A. Monti, ed., Springer London, London, pp. 113–127.
- [12] “Container Handbook” [Online]. Available: [https://www.containerhandbuch.de/chb\\_e/stra/index.html](https://www.containerhandbuch.de/chb_e/stra/index.html). [Accessed: 06-Jun-2023].
- [13] “20 Foot Shipping Containers | Dimensions,” *ModuGo* [Online]. Available: <https://modugo.com/20-ft-shipping-container-dimensions/>. [Accessed: 06-Jun-2023].



- [14] “Intermodal System Maps & Directories | Intermodal” [Online]. Available: <https://www.intermodal.org/resource-center/intermodalsystem>. [Accessed: 06-Jun-2023].
- [15] Jiskra, A., Gwozdz, M., Sliwa, J., and Liang, H., “Feasibility of Chip Energy’s Biofuel Production Network.”
- [16] “Coal - Classification” [Online]. Available: [https://www.engineeringtoolbox.com/classification-coal-d\\_164.html](https://www.engineeringtoolbox.com/classification-coal-d_164.html). [Accessed: 31-Mar-2023].
- [17] “Natural Gas Density Calculator | Unitrove” [Online]. Available: <https://www.unitrove.com/engineering/tools/gas/natural-gas-density>. [Accessed: 06-Jun-2023].
- [18] “AC Current Transducer: 1-Phase, Split Core, 0-10, 0-20, or 0-50A Selectable Sensing Range (PN# ACT050-42L-S) | AutomationDirect” [Online]. Available: [https://www.automationdirect.com/adc/shopping/catalog/sensors\\_-z-\\_encoders/current\\_-a-\\_voltage\\_sensors\\_\(ac\\_-a-\\_dc\)/1-phase\\_ac\\_current\\_transducers/act050-42l-s?gclid=CjwKCAjwsvujBhAXEiwA\\_UXnAAG9j9XOYKmioInTE3ZDCpMvXPptSZIZyZrM0sEzyOzv52RSW0yFRoCGdQQA\\_VD\\_BwE](https://www.automationdirect.com/adc/shopping/catalog/sensors_-z-_encoders/current_-a-_voltage_sensors_(ac_-a-_dc)/1-phase_ac_current_transducers/act050-42l-s?gclid=CjwKCAjwsvujBhAXEiwA_UXnAAG9j9XOYKmioInTE3ZDCpMvXPptSZIZyZrM0sEzyOzv52RSW0yFRoCGdQQA_VD_BwE). [Accessed: 06-Jun-2023].
- [19] Winebrake, J. J., Corbett, J. J., Falzarano, A., Hawker, J. S., Korfmacher, K., Ketha, S., and Zilora, S., 2008, “Assessing Energy, Environmental, and Economic Tradeoffs in Intermodal Freight Transportation,” *J. Air Waste Manag. Assoc.*, **58**(8), pp. 1004–1013.
- [20] Vanek, F., 2019, “Mode and Commodity Perspectives on U.S. Freight Energy Consumption and CO2 Emissions: Insights and Directions for Improvement,” *Int. J. Sustain. Transp.*, **13**(10), pp. 741–760.
- [21] Franz, R. D., 2009, “Corn Stover Densification Using an Auger Compactor,” Master of Science, Iowa State University, Digital Repository.
- [22] “Amazon.Com: Best Harvest Hay Bale Sampler Probe, 36in Depth, Drill-Type for Sampling Hay Bales. 42in Overall Length. Includes Bagging Attachment : Patio, Lawn & Garden” [Online]. Available: [https://www.amazon.com/Best-Harvest-Drill-Type-Sampling-Attachment/dp/B096QRMPF3/ref=sr\\_1\\_1?keywords=%E2%80%A2+Hay+Bale+Sampler+Probe%2C+36%22+Depth%2C+Drill-Type+for+Sampling+Hay+Bales&qid=1670343127&sr=8-1](https://www.amazon.com/Best-Harvest-Drill-Type-Sampling-Attachment/dp/B096QRMPF3/ref=sr_1_1?keywords=%E2%80%A2+Hay+Bale+Sampler+Probe%2C+36%22+Depth%2C+Drill-Type+for+Sampling+Hay+Bales&qid=1670343127&sr=8-1). [Accessed: 06-Jun-2023].
- [23] “Gas Powered Core Sampling Kit,” AMS Inc [Online]. Available: <https://www.ams-samplers.com/gas-powered-core-sampling-kit/>. [Accessed: 06-Jun-2023].
- [24] “Aluminum Blast Gate, with Galvanized Steel Slide, Duct Size 12, 11-13/16" Male OD | McMaster-Carr” [Online]. Available: <https://www.mcmaster.com/1788K19/>. [Accessed: 06-Jun-2023].
- [25] “Heavy Duty Hinge with Holes, Low-Carbon Steel, 3" x 2" Door Leaf, 0.375" Leaf Thickness | McMaster-Carr” [Online]. Available: <https://www.mcmaster.com/1852A59/>. [Accessed: 06-Jun-2023].
- [26] “Tight-Hold Draw Latch, with Safety Catch, 304 Stainless Steel, 3-15/16" Long x 2-1/16" Wide | McMaster-Carr” [Online]. Available: <https://www.mcmaster.com/1794A64/>. [Accessed: 06-Jun-2023].

- [27] Goodey, R. J., Brown, C. J., and Rotter, J. M., 2017, "Rectangular Steel Silos: Finite Element Predictions of Filling Wall Pressures," *Eng. Struct.*, **132**, pp. 61–69.
- [28] Crawford, N. C., Ray, A. E., Yancey, N. A., and Nagle, N., 2015, "Evaluating the Pelletization of 'Pure' and Blended Lignocellulosic Biomass Feedstocks," *Fuel Process. Technol.*, **140**, pp. 46–56.
- [29] "Auger RPM Calculator - Sudenga Industries Inc. | Made in the USA," Sudenga Ind. Inc [Online]. Available: <https://sudenga.com/resources/calculating-auger-rpm/>. [Accessed: 06-Jun-2023].
- [30] "Surface-Mount Hinge with Holes, Brass, Nonremovable Pin, 3/4" x 5/16" Door Leaf | McMaster-Carr" [Online]. Available: <https://www.mcmaster.com/1603A2/>. [Accessed: 06-Jun-2023].
- [31] "Draw Latch, Screw on, 304 Stainless Steel, 1-7/8" Long x 1-3/8 Wd | McMaster-Carr" [Online]. Available: <https://www.mcmaster.com/1889A34/>. [Accessed: 06-Jun-2023].